8-9-2019

Remote sensing of colored dissolved organic matter using unmanned aerial systems and assessment of the influence of dissolved organic matter on the oyster reefs in the western Mississippi sound

Sudeera Wickramarathna Galapita Pallayapelage

Remote sensing of colored dissolved organic matter using unmanned aerial systems and assessment of the influence of dissolved organic matter on the oyster reefs in the western Mississippi sound

By

Sudeera Wickramarathna Galapita Pallayapelage

A Thesis
Submitted to the Faculty of
Mississippi State University
in Partial Fulfillment of the Requirements
for the Degree of Master of Science
in Geoscience
in the Department of Geosciences

Mississippi State, Mississippi

August 2019

Remote sensing of colored dissolved organic matter using unmanned aerial systems and assessment of the influence of dissolved organic matter on the oyster reefs in the western Mississippi sound

By

Sudeera Wickramarathna Galapita Pallayapelage

Approved:

_____

Padmanava Dash
(Major Professor)

_____

Andrew E. Mercer
(Committee Member)

_____

Varun G. Paul
(Committee Member)

_____

Renee M. Clary
(Graduate Coordinator)

_____

Rick Travis
Dean
College of Arts & Sciences

Name: Sudeera Wickramarathna Galapita Pallayapelage

Date of Degree: August 9, 2019

Institution: Mississippi State University

Major Field: Geoscience

Major Professor: Padmanava Dash

Title of Study: Remote sensing of colored dissolved organic matter using unmanned aerial systems and assessment of the influence of dissolved organic matter on the oyster reefs in the western Mississippi sound

Pages in Study: 79

Candidate for Degree of Master of Science

Oyster reefs in the western Mississippi Sound (WMS) are dependent on the salinity moderation by freshwater input. However, freshwater brings in high amount of pollutants, which affect the oysters negatively. Oyster diebacks happened as a result of hypoxia caused by excessive organic matter input to WMS in summer 2017. Colored dissolved organic matter (CDOM) is widely used as a proxy for determining organic matter distribution. In this study, hyperspectral and multispectral remote sensing data collected using unmanned aerial systems and *in situ* CDOM data were used to develop algorithms in order to retrieve CDOM remotely. Collected physical and biogeochemical parameters were used to understand the carbon fluxes regulating the quality and quantity of CDOM. Developed algorithms showed high accuracy after accounting for seasonal variations of CDOM. Further, seasonal induced photodegradation, photosynthesis, calcification, and exchange of CO_2 were identified as possible factors that affect the carbon dynamics in the study area.

ACKNOWLEDGEMENTS

I would like to express my sincere gratitude to my advisor, Dr. Padmanava Dash, for giving me the opportunity to pursue my master's degree and patiently guiding me with great enthusiasm, and introducing me to the field of remote sensing and water quality. Without his continuous guidance and support, this thesis would not have been possible. Also, I would like to offer special thanks to my committee, Dr. Andrew E. Mercer and Dr. Varun Paul, for their tremendous support, guidance, and for providing me helpful comments and suggestions throughout my thesis work.

I would like to thank my fellow graduate students who supported me during the field trips and for encouraging me. Especially, I would like to thank Sankar, Landon, Wondim, and Rusch for their support during my thesis research. Also, I would like to give a special thanks to the faculty and staff of the Department of Geosciences at Mississippi State University for all their help. I thank the Department of Geosciences for providing me teaching assistantship support and for providing laboratory facilities.

This project was paid for with federal funding from the Department of the Treasury under the Resources and Ecosystems Sustainability, Tourist Opportunities, and Revived Economies of the Gulf Coast States Act of 2012 (RESTORE Act). The statements, findings, conclusions, and recommendations do not necessarily reflect the views of the Department of the Treasury.

TABLE OF CONTENTS

LIST OF TABLES

LIST OF FIGURES

CHAPTER I

INTRODUCTION

Organic matter is compositionally heterogeneous, and ubiquitous in both aquatic and terrestrial environments (O'Melia et al., 2006). In terrestrial environment, organic matter is predominantly stored in organisms, plants, and surface soils (Post, 1993; Eswaran et al., 1993). In the aquatic environment, organic matter occurs either in dissolved or particulate form (Bolan et al., 2011). Dissolved organic matter (DOM) forms a large portion of organic carbon pool in aquatic environments (Hedges et al., 1992; Hansell et al., 2009) and considered as the primary energy source for aquatic microorganisms (Moran et al., 2000). However, excess amount of DOM in the aquatic environment causes many water quality issues such as bottom water hypoxia (Hetland and DiMarco, 2008), acidification (Benner, 2002), harmful algal blooms (Heisler et al., 2008), reduction in light penetration (D'sa and DiMarco, 2009), and also facilitates transportation of toxic elements and heavy metals (Stanley et al., 2012). Hence, monitoring and management of DOM is essential for the sustainability of the aquatic resources.

DOM is a complex mixture of different types of organic molecules (e.g., humic and fulvic acid, carbohydrates and proteins) formed by elements such as carbon, hydrogen, oxygen, nitrogen, phosphorus, and sulfur (Coble et al., 1998; Tiwari et al., 2011; Chaichitehrani et al., 2013; Findlay and Parr, 2017). Dissolved organic carbon (DOC) is the predominant constituent in DOM pool with other nutrients such as dissolved organic nitrogen (DON), dissolved organic phosphorus (DOP), and dissolved organic sulfur (DOS) (Cleveland et al., 2004). Further, colored dissolved

organic matter (CDOM) is considered as the optically active fraction of the DOM pool also used as a proxy to evaluate quality and quantity of DOC and DOM in aquatic systems (Del Castillo et al., 1999; Jaffe' et al., 2008).

Spectrofluorometric analysis such as Fourier transform ion-cyclotron resonance-mass spectrometry (FTICR-MS) or Nuclear Magnetic Resonance (NMR) spectroscopy provides detailed information on the composition and concentrations of all the organic compounds constituting DOM in a water sample (Fellman et al., 2010, 2009b; Jaffé et al., 2008; Kaushal and Lewis, 2005; Lu et al., 2013). Such information is useful to determine not only the source, transportation pathways, and fate of DOM, but also it is useful for inferring the biogeochemical processes undergoing in a water body and in the watershed that is draining to the waterbody (Jaffe' et al., 2008; Sankar et al., 2019). However, characterization of DOM using FTICR-MS or NMR is very expensive and time-consuming. DOC, the dominant component of DOM, can be measured cost-effectively in a laboratory in a short time period. Further, CDOM could be measured even more easily using optical instruments in a very effective manner (Coble et al., 2004). Since CDOM is highly correlated to total DOM and DOC, measurement of CDOM can provide important insights into DOM dynamics (Paerl et al., 2006). All these laboratory characterizations of DOM requires water sample collection, which is labor intensive and expensive. Water samples from a few locations may not represent the variability of the natural environment. As opposed to point sampling, use of remote sensing technique is economical and it provides synoptic views with coverages that is unmatched by data collection at fixed stations. Being an optically active constituent, CDOM dynamics can be studied using remote sensing techniques. Thus, remote sensing techniques can be used to monitor the spatial and temporal distribution of DOM dynamics in an efficient way.

In order to manage the DOM dynamics in an aquatic setting, it is essential to understand its source, transport, fate, and interrelationship with other physical and biogeochemical parameters. The DOM can be either allochthonous (i.e. originate from terrestrial sources) or autochthonous (i.e. originate from *in-situ* primary production) (Twardowski and Donaghay 2001; Rochelle-Newall and Fisher, 2002). Rivers and streams transport DOM to the ocean. During transportation, microbial activity may convert the DOM to be more labile or may retain a lot of recalcitrant DOM. DOM could also form complexes with trace elements and heavy metals during transportation. Additionally, photochemical reactions in the presence of sunlight could also alter the DOM significantly (Sankar et al., 2019). Both allochthonous and autochthonous DOM undergo significant microbial activity in the water body. Higher DOM concentrations in the water body leads to increased microbial activity. Unlike surface waters where oxygen could be replenished from the atmosphere, in the absence of mixing, hypoxic or anoxic conditions can develop in the bottom waters because of increased microbial activity due to higher DOM concentrations. Along the similar line, the composition of DOM has also a significant bearing on the bottom water hypoxia or anoxia since labile DOM are more bioavailable than recalcitrant DOM. Increased microbial activity also produces inorganic carbon through microbial respiration decreasing the pH. Temperature and salinity also have significant influence on the transformation of DOM. Hence, measurement of a suite of parameters help in understanding the physical and biogeochemical processes affecting the DOM dynamics. Since, DOM dynamics is closely related to health of oyster reefs, determination of DOM dynamics not only helps in understanding the processes affecting the oyster reefs but also provides valuable insights into management of water quality for the betterment of the oyster reefs.

The main goal of the this thesis research was to devise a procedure for effective DOM monitoring and determine the physical and biogeochemical processes controlling the DOM dynamics to aid in management of water quality over the Pass Christian and Henderson Point oyster reefs in western Mississippi sound. Collection of remotely sensed data using unmanned aerial systems and laboratory measurement of CDOM were used to develop remote sensing algorithms for estimating CDOM from remotely sensed data. Measurements of CDOM along with water quality parameters such as salinity, pH, temperature, DO, DOC, dissolved inorganic carbon, and total alkalinity were used to evaluate the DOM dynamics in the study area. The first project (Chapter II) covers the development of remote sensing algorithms for estimating CDOM using remotely sensed data and the second project (Chapter III) entails the biogeochemical processes controlling DOM dynamics and its influence on the water quality of the Pass Christian and Henderson Point oyster reefs in the western Mississippi sound.

1.1 References

Benner, R., Pakulski, J.D., McCarthy, M., Hedges, J.I. and Hatcher, P.G., 1992. Bulk chemical characteristics of dissolved organic matter in the ocean. *Science*, *255*(5051), pp.1561-1564.

Bolan, N.S., Adriano, D.C., Kunhikrishnan, A., James, T., McDowell, R. and Senesi, N., 2011. Dissolved organic matter: biogeochemistry, dynamics, and environmental significance in soils. In *Advances in agronomy* (Vol. 110, pp. 1-75). Academic Press.

Chaichitehrani, N., D'sa, E.J., Ko, D.S., Walker, N.D., Osburn, C.L. and Chen, R.F., 2013. Colored dissolved organic matter dynamics in the northern Gulf of Mexico from ocean color and numerical model results. Journal of Coastal Research, 30(4), pp.800-814.

Coble, P., Hu, C., Gould Jr, R.W., Chang, G. and Wood, A.M., 2004. Colored Dissolved Organic Matter in the Coastal Ocean: An Optical Tool for Coastal Zone Environmental Assessment & Management (No. NRL/JA/7330-04-15). Naval Research Lab Stennis Space Center Ms Oceanography Div.

Cleveland, C.C., Neff, J.C., Townsend, A.R. and Hood, E., 2004. Composition, dynamics, and fate of leached dissolved organic matter in terrestrial ecosystems: results from a decomposition experiment. *Ecosystems*, *7*(3), pp.175-285.

Del Castillo, C.E., Coble, P.G., Morell, J.M., Lopez, J.M. and Corredor, J.E., 1999. Analysis of the optical properties of the Orinoco River plume by absorption and fluorescence spectroscopy. Marine Chemistry, 66(1-2), pp.35-51.

D'Sa, E.J. and DiMarco, S.F., 2009. Seasonal variability and controls on chromophoric dissolved organic matter in a large river-dominated coastal margin. *Limnology and Oceanography*, *54*(6), pp.2233-2242.

Eswaran, H., Van Den Berg, E. and Reich, P., 1993. Organic carbon in soils of the world. *Soil science society of America journal*, *57*(1), pp.192-194.

Fellman, J.B., Hood, E., Edwards, R.T., D'Amore, D.V. 2009. Changes in the concentration, biodegradability, and fluorescent properties of dissolved organic matter during stormflows in coastal temperate watersheds. J. Geophys. Res. 114, 1–14.

Fellman, J.B., Hood, E., Spencer, R.G.M., 2010. Fluorescence spectroscopy opens new windows into dissolved organic matter dynamics in freshwater ecosystems: A review. Limnol. Oceanogr. 55, 2452–2462.

Findlay, S.E. and Parr, T.B., 2017. Dissolved organic matter. In Methods in Stream Ecology (pp. 21-36). Academic Press.

Hansell, D.A., Carlson, C.A., Repeta, D.J., and Schlitzer, R., 2009. Dissolved organic matter in the ocean: A controversy stimulates new insights: oceanography, 22(4), pp.202-211.

Hedges, J.I., 1992. Global biogeochemical cycles: progress and problems. Marine Chemistry, 39(1-3), pp.67-93.

Heisler, J., Glibert, P.M., Burkholder, J.M., Anderson, D.M., Cochlan, W., Dennison, W.C., Dortch, Q., Gobler, C.J., Heil, C.A., Humphries, E. and Lewitus, A., 2008. Eutrophication and harmful algal blooms: a scientific consensus. *Harmful algae*, *8*(1), pp.3-13.

Hetland, R.D. and DiMarco, S.F., 2008. How does the character of oxygen demand control the structure of hypoxia on the Texas–Louisiana continental shelf?. Journal of Marine Systems, 70(1-2), pp.49-62.

Jaffé, R., McKnight, D., Maie, N., Cory, R., McDowell, W.H., Campbell, J.L., 2008. Spatial and temporal variations in DOM composition in ecosystems: The importance of long-term monitoring of optical properties. J. Geophys. Res. 113, 1–15.

Kaushal, S.S. and Lewis, W.M., 2005. Fate and transport of organic nitrogen in minimally disturbed montane streams of Colorado, USA. Biogeochemistry, 74(3), pp.303-321.

Lu, Y., Bauer, J.E., Canuel, E.A., Yamashita, Y., Chambers, R.M. and Jaffé, R., 2013. Photochemical and microbial alteration of dissolved organic matter in temperate headwater streams associated with different land use. *Journal of Geophysical Research: Biogeosciences*, *118*(2), pp.566-580.

Moran, M.A., Sheldon Jr., W.M., Zepp, R.G., 2000. Carbon loss and optical property changes during long-term photochemical and biological degradation of estuarine dissolved organic matter. Limnol. Oceanogr. 45, 1254–1264.

O'Melia, C.R., 2006. Fundamentals of particle stability. In *Interface Science and Technology* (Vol. 10, pp. 317-362). Elsevier.

Paerl, H.W., Valdes, L.M., Peierls, B.L., Adolf, J.E. and Lawrence Jr, W.H., 2006. Anthropogenic and climatic influences on the eutrophication of large estuarine ecosystems. Limnology and Oceanography, 51(1part2), pp.448-462.

Post, W.M., 1993. Organic carbon in soil and the global carbon cycle. In The Global Carbon Cycle (pp. 277-302). Springer, Berlin, Heidelberg.

Rochelle-Newall, E.J. and Fisher, T.R., 2002. Production of chromophoric dissolved organic matter fluorescence in marine and estuarine environments: an investigation into the role of phytoplankton. Marine Chemistry, 77(1), pp.7-21.

Sankar, M.S., Dash, P., Singh, S., Lu, Y., Mercer, A.E. and Chen, S., 2019. Effect of photo-biodegradation and biodegradation on the biogeochemical cycling of dissolved organic matter across diverse surface water bodies. *Journal of Environmental Sciences*, *77*, pp.130-147.

Stanley, E.H., Powers, S.M., Lottig, N.R., Buffam, I. and Crawford, J.T., 2012. Contemporary changes in dissolved organic carbon (DOC) in human-dominated rivers: is there a role for DOC management?. Freshwater Biology, 57, pp.26-42.

Tiwari, S.P. and Shanmugam, P., 2011. An optical model for the remote sensing of coloured dissolved organic matter in coastal/ocean waters. *Estuarine, Coastal and Shelf Science*, *93*(4), pp.396-402.

Twardowski, M.S. and Donaghay, P.L., 2001. Separating in situ and terrigenous sources of absorption by dissolved materials in coastal waters. Journal of Geophysical Research: Oceans, 106(C2), pp.2545-2560.

CHAPTER II

ASSESSMENT OF COLOURED DISSOLVED ORGANIC MATTER USING HYPERSPECTRAL AND MULTISPECTRAL SENSORS OVER THE OYSTER REEFS IN THE WESTERN MISSISSIPPI SOUND

2.1 Introduction

Dissolved organic carbon (DOC), one of the largest carbon pools in the environment, is considered as the major component of dissolved organic matter (DOM) (Carlson et al., 1994). Colored dissolved organic matter (CDOM), the optically active component of the DOM pool, is used as a proxy to measure DOC using remote sensing techniques (Del Castillo et al., 1999; Jaffe' et al., 2004). Carbon fluxes in estuarine and coastal systems are complex in nature, and estimation of carbon budgets is arduous with traditional scientific methods (Bauer et al., 2013). Synoptic observations from space provide broad scale observations which can capture the biogeochemical exchanges in ocean systems with high magnification both spatially and temporally. In coastal oceans, the majority of total organic carbon is DOC (80-90%), which is known as the "great modulator" that influences other physicochemical variables (Prairie, 2008). Since DOC is highly correlated with CDOM, effects of DOC can be identified with the estimation of CDOM in waterbodies with remote sensing approaches (Laanen, 2007). During the past few decades, a considerable number of remote sensing approaches have been developed to estimate CDOM using remotely sensed data. Majority of the algorithms have been developed by utilizing spaceborne remote sensing instruments (Pierson and Strömbeck, 2000; Siegel et al., 2000; Zhu et al. 2011).

Although satellite remote sensing is very useful, sometimes can be limited by spatial and temporal resolution, atmospheric interferences, and/or cloud cover (Ozesmin and Bauer, 2002; Kutser et al., 2005; Bhardwaj et al., 2016). There are some satellite sensors which provide remotely sensed data with high spatial resolution (e.g., Geoeye-1 and WorldView-4) but these imagery are expensive and limited by temporal resolution for environmental monitoring purposes (Nebiker et al., 2008). Aerial photography using aeroplanes can also be used to obtain high-resolution imagery with less interference from the atmosphere, but it is still expensive and it needs an airport nearby and a significant amount of logistical support (Alesheikh et al., 2007).

Compared to satellite remote sensing and aerial photography using aeroplanes, miniature and lightweight airborne platforms, unmanned aerial systems (UASs), provide a new generation of inexpensive remote sensing platforms with high spatial and temporal resolution capabilities for the collection of a wide range of remote sensing data (Nebiker et al., 2008; Bhardwaj et al., 2016). Compared to traditional remote sensing approaches, UASs have many advantages. For example, UASs can utilize various types of payloads and cameras based on desired data acquisition (e.g., multispectral, hyperspectral, thermal, and microwave etc.). Depending on the necessity, UASs can change the flying heights and viewing angles to collect high spatial resolution data over a study area. Further, UASs can be flown at the time of need and as frequently as the data is needed. Another advantage of the use of UASs is they can be flown under the cloud providing usable remotely sensed data when satellite borne sensors fail to provide visible and infrared remote sensing data (Bhardwaj et al., 2016). However, as a discipline UAS remote sensing is still in its infancy. Hence, development of methods for processing of UAS remote sensing data for obtaining high quality scientific data is necessary.

Estimation of water quality parameters using remote sensing is relatively easy in the open ocean waters because the optical properties in the open ocean are mainly determined by phytoplankton and their derived products (Smith and Baker 1978; Mobley, 2004). In contrast, light attenuation in coastal waters are considerably higher and optically more complex as compared to the open oceanic waters. This higher complexity is because terrestrial runoff brings in high amount of particulate and dissolved organic and inorganic matter to the coastal waters (Woodruff et al., 1999). Also, because of terrestrial-derived nutrients and bottom resuspension, phytoplankton populations are typically higher in the coastal waters. Thus, the remote sensing instruments measure signal from all these substances in coastal waters including signal from chlorophyll-*a* (chl-*a*), total suspended solids (TSS), CDOM, and the water itself (Bukata et al., 1995; Koponen et al., 2007). Therefore, estimation of CDOM in coastal waters is arduous with the presence of these other optically active constituents. Hence, most of the remote sensing algorithms have some amount of uncertainties because of these optically active constituents other than CDOM, which append noises to the water leaving CDOM signal (Tehrani et al., 2013; Lee et al., 2010; Werdell et al., 2013). Thus, estimation of CDOM using remotely sensed data should be performed carefully by choosing wavelength bands for maximizing the signal strength from CDOM while minimizing the signal from other undesired water quality parameters.

The primary goal of this study was to develop remote sensing algorithms for estimating CDOM using hyperspectral and multispectral data collected using UASs. The primary questions addressed in this study are: 1) - Is it possible to estimate CDOM using UAS imagery with reasonable accuracy? 2) What is the relative accuracy of estimated CDOM using multispectral data in compared to hyperspectral data? 3) Which bands are optimal for CDOM estimation? 4) What functional form of the algorithm is optimal for estimating CDOM?

2.2 Methods and materials

2.2.1 Study area

Commercially and ecologically important productive oyster reefs are located along the western Mississippi Sound (WMS) (Figure 2.1). These oyster reefs are an important asset for the state of Mississippi and the United States. Henderson Point and Pass Christian oyster reefs together make the largest oyster reef along WMS in northern Gulf of Mexico. However, most of the oyster beds located along the WMS are facing dire problems due to occasional high freshwater inputs, terrestrial runoff bringing high amounts of organic matter, harmful algal blooms, hypoxia, pathogen contamination, storms, hurricanes, coastal developments, and oil spills from onshore and offshore oil rigs (La Peyre et al., 2012; McCrea-Strub et al., 2011; Pollack et al., 2011). Two blackwater rivers, Jordan River (JR) and Wolf River (WR) provide freshwater input to the study region through Bay St. Louis (BSL), a semi-closed shallow (avg. depth of 1.5m) bay. Apart from these river inputs, freshwater from outflows of the Pearl River influences WMS along with seawater from the Gulf of Mexico with wind mixing and regional circulations. Recently, Ho et al. (2019) reported the possibility of submarine groundwater discharge (SGD) influencing the water quality of WMS. Further, during flood situations, the diverted Mississippi River water through the Bonnet Carre Spillway via Lake Pontchartrain brings in freshwater and a high concentration of nutrients that sometimes proves detrimental to the oysters. The continued decline in oyster reefs has become a significant issue in commercial fisheries production and has caused countless restoration efforts that are being carried out globally (Beck et al., 2011; La Peyre et al., 2012).

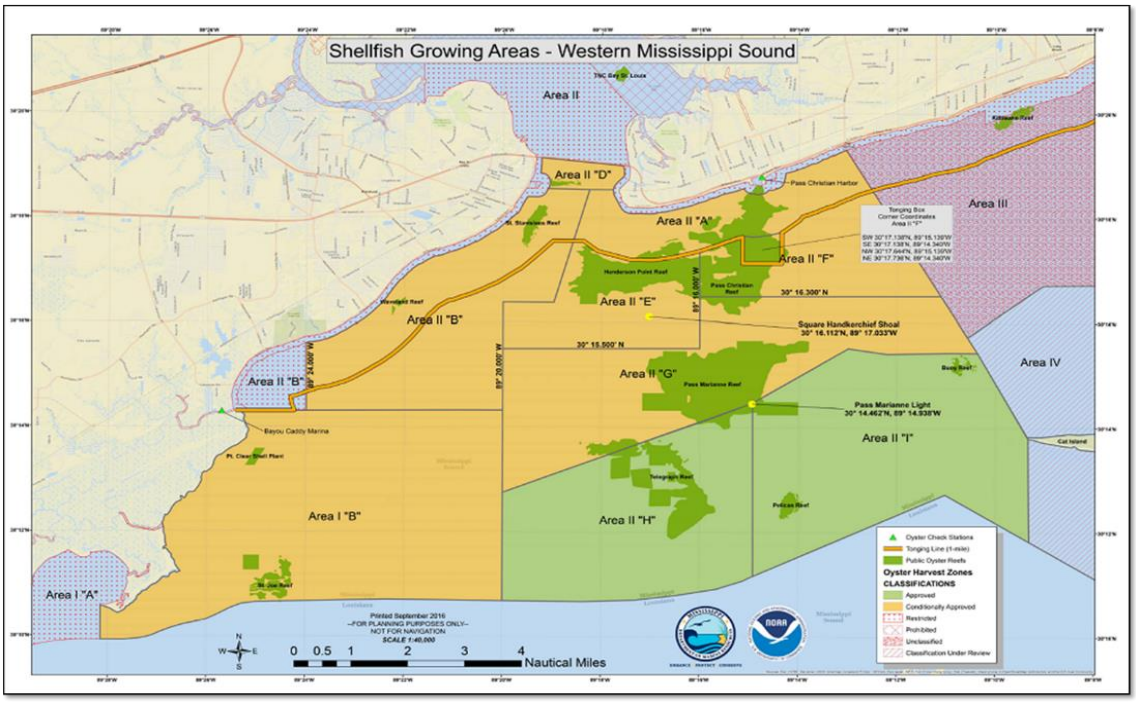

Figure 2.1 Map of western Mississippi Sound. The largest green polygon represents the Henderson Point and Pass Christian Oyster Reefs. (Source: MDMR, 2013 The Oystermen's Guide to Mississippi Gulf Coast Oyster Reefs)

Previous studies suggested hypoxia (Soletchnik et al., 1998; Soletchnik et al., 2007), salinity variations (Lipovsky and Chew, 1972), eutrophication (Gray et al., 2002), and sedimentation as possible explanations for mass mortality of oysters in NGoM region. Most recently, oyster diebacks happened as a result of hypoxia caused by excessive organic matter input to the WMS in summer 2017 (MDMR, personal communication). Hypoxic conditions (dissolved oxygen <2 mg/L) occur as a result of entering excessive organic matter into the water column, since degradation of organic matter can consume a significant amount of DO in the water column (Gray et al., 2002). Malham et al. (2009) showed a direct, strong influence of terrestrially derived DOM and mass mortalities of oysters. Thus, CDOM serve as a very useful indicator of DOM affecting oyster health (Blough and Del Vecchio, 2002).

2.2.2 Water sample, *in situ* data, and unmanned aerial systems imagery collection

Four sampling trips one week each were carried out in the months of March, May, June, and July 2018, respectively, and a total of 45 water samples were collected (Fig. 2.2, Table 2.1). Surface water samples were collected in acid-washed 1-liter clean Nalgene bottles using a sampling stick from a non-agitated water surface. Samples were stored in a cooler with ice and transported to the laboratory within 2 h of collection. The *in situ* data collection included *in situ* remote sensing reflectance measurements using a GER 1500 spectro-radiometer (Spectravista Inc., NY), backscattering and fluorescence measurements using two Eco-Triplets (Wetlabs Inc., OR), and physical parameter measurements using a calibrated Hanna multiparameter probe (HI9828, Hanna Instruments, RI). A DJI M600 hexacopter unmanned aerial vehicle (DJI Inc., Washington D. C., USA) outfitted with two sensors, a nano-hyperspec hyperspectral sensor (Headwall Photonics Inc., Bolton, MA, USA) and a RedEdge multispectral sensor (Micasense Inc., Seattle, WA, USA) was flown at each site to collect UAS imagery covering 0.5 sq. mi. rectangular area around each site.

Table 2.1 Summary of field data collection

Sampling Trips	Date	Water Samples	Usable Radiometer Data	Unmanned Aerial Systems flights
1	6-8 March 2018	9	5	9
2	7-12 May 2018	19	15	19
3	18-20 June 2018	9	9	9
4	16-20 July 2018	7	0*	7

***Data collection was not successful**

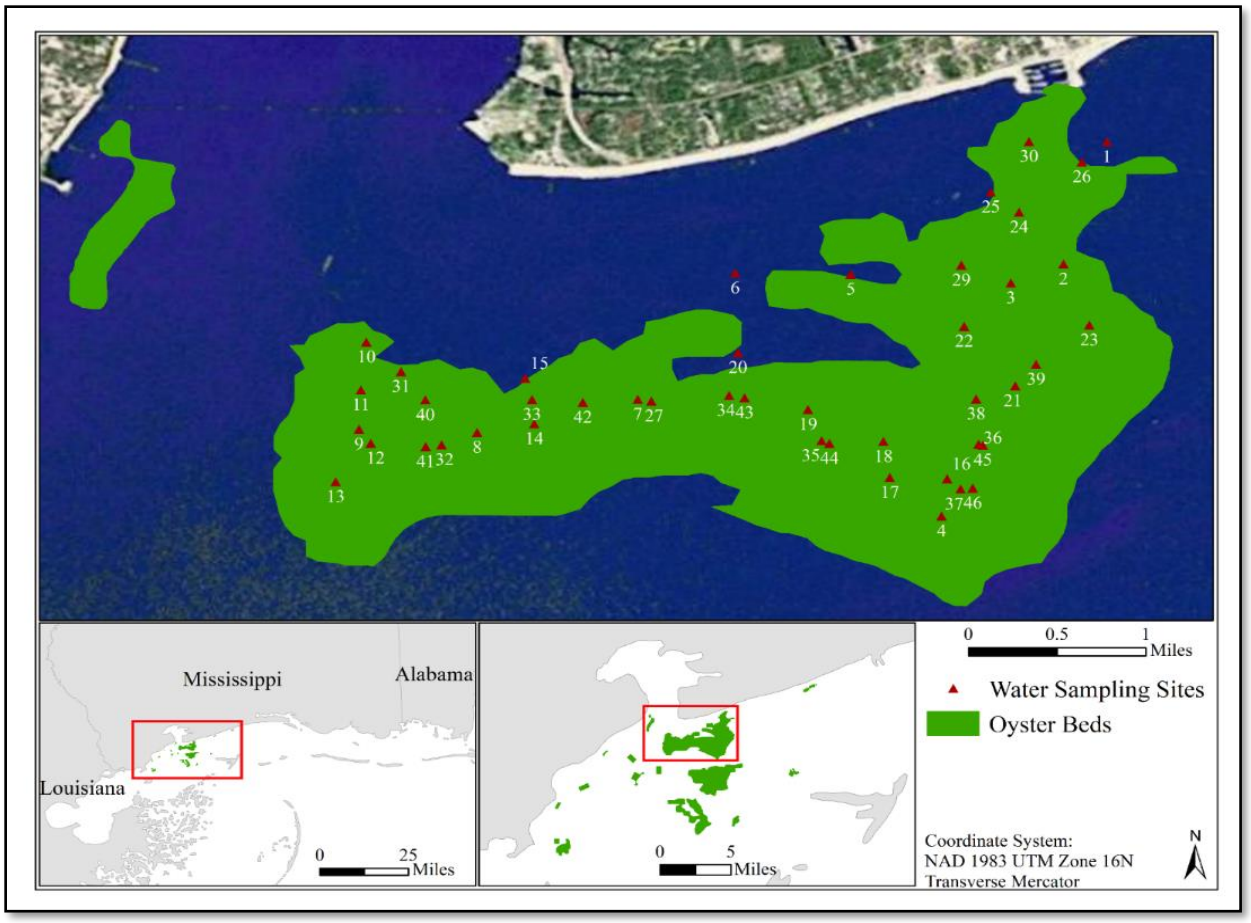

Figure 2.2 Map of the study area. Red triangles represent the sampling locations.

2.2.3 Water level and discharge

Water level and discharge data were downloaded from the United States Geological Survey (USGS) site numbers 02481521 and 02481660 for Wolf River (WR) and Jourdan River (JR), respectively. The freshwater replacement time in the BSL was estimated as an average of 4.1 days based on the estimates of freshwater replacement from both WR and JR rivers (Sawant, 2009). However, it must be recognized that the winds and diurnal tidal cycles will have a pronounced effect on water residence times in BSL. This is among the shortest residence time in the NGoM estuaries (Solis and Powell, 1999). Since the water sampling in the western Mississippi Sound was

carried out for multiple days at a time, for determining the water level and discharge for the first field trip date, the average of water level and discharge of 4 days preceding the first field trip was calculated. Similarly, the water level and discharge for the second date was determined by calculating the average of water level and discharge of 4 days preceding the second field trip date. The water level and discharge for subsequent field trip dates were calculated in a similar manner. Finally, taking an average of all these mean water levels and discharges provided the average water level and discharge for one entire field trip. The average water level and discharge for each field trip were calculated in this fashion with one value each for the March, May, June, and July field trips.

2.2.4 Analytical methods

2.2.4.1 CDOM absorption coefficient analysis

50 mL of the collected water samples from each site were filtered using Nuclepore membrane filters with 0.2 µm pore size under low vacuum in the laboratory. Filtered samples were stored at 4 ^{o}C in acid cleaned, pre-combusted amber colored glass bottles. On the day of absorbance measurement, samples were kept outside of the refrigerator to reach ambient room temperature and then the absorbance of CDOM was measured using a double beam Perkin Elmer Lambda 850 spectrophotometer (Waltham, MA, USA) with a 150 mm spectralon coated integrating sphere. A quartz cuvette with 1 cm path length was used to measure the absorbance (A) from 400nm to 750nm with 2 nm increments. Absorbance values were corrected for scattering and baseline fluctuations by subtraction of the mean value of the measured absorbance from 700 - 750 nm from the absorbance at each wavelength. Next, the absorbance spectra of Nanopure Milli-Q water were

subtracted for each wavelength. Finally, the CDOM absorption coefficient ($a_{CDOM}(\lambda)$) was calculated by following Hu et al. (2002) as

$$a_{CDOM}(\lambda) = \frac{2.303[A_{CDOM}(\lambda)]}{l} \quad (2.1)$$

where l is the path length of the cuvette and λ is the wavelength in nm. $A_{CDOM}(\lambda)$ is the absorbance value measured by the spectrophotometer.

Using a_{CDOM} values from 400-550 nm, the spectral slopes of CDOM (S_{CDOM}) for each site were determined using nonlinear least squares regression (Chen et al., 2007). The spectral slopes were used along with a_{CDOM} at 440 to obtain a smooth a_{CDOM} spectra for each site following:

$$a_{CDOM}(\lambda) = a_{CDOM}(\lambda_0)\, e^{-S_{CDOM}(\lambda-\lambda_0)} \quad (2.2)$$

where, $a_{CDOM}(\lambda_0)$ is the CDOM absorption coefficient at a reference wavelength (e.g.,440 nm), and λ is the wavelength at which CDOM absorption coefficients were desired (e.g., 400,412, and 440 nm). Zhu et al., 2014 used a_{CDOM} at 412 nm or 440 nm for expressing CDOM concentrations in water. In this study, a_{CDOM} at 400, 412, and 440 nm were used to describe the amount of CDOM in the water samples.

2.2.4.2 Dissolved Organic Carbon analysis

For dissolved organic carbon (DOC) analysis, aliquots of water samples were filtered using Nuclepore membrane filters with 0.2 µm pore size under low vacuum and the filtrates were stored in 20ml HDPE bottles at -80°C. DOC concentrations were measured using a SHIMADZU® TOC-TNM1 total organic carbon-total nitrogen analyzer equipped with an ASI-V auto ampler as described in Shang et al. (2018).

2.2.4.3 Chlorophyll *a* analysis

100 ml of water samples in duplicates were filtered through 47 mm diameter GF/F filters (Whatman®, 0.7 µm), filter papers were folded and covered with aluminum foil and stored in 80°C. On the day of the chlorophyll *a* (chl-*a*) analysis, extraction of chl-*a* was carried out using 90% acetone according to the protocols mentioned in Herbland et al. (1985). Extracted chl-*a* - samples were measured using a Horiba FluoroMax-4® spectrofluorometer (Edison, NJ, USA).

2.2.5 Radiometric data

2.2.5.1 Above-water measurements

In situ radiometric data were collected from above the water surface by avoiding the sun glint and shadow of the boat at each site. Water leaving spectral radiance was measured using a GER 1500 a portable field spectroradiometer (Spectravista Inc., NY), which covers the UV, Visible, and NIR wavelengths from 286.90-1089.62 nm with ~1.85 nm spectral resolution. The water-surface radiance (L_{water}), sky radiance (L_{sky}), and radiance from a 99% Labsphere reference Spectralon plaque (L_{plaque}) were obtained. Three water leaving radiance values were taken and averaged. Remote-sensing reflectance (R_{rs}) were derived by following Mueller et al. (2003) and Mobley (1999) as following:

$$E_{d}=\pi \times L_{Plaque} \times 0.99 \quad (2.3)$$

$$R_{rs}=\frac{L_{water} - (\rho \times L_{sky})}{E_{d}} = \frac{Upwelling\ Radiance}{Downwelling\ Irradience} \quad (2.4)$$

Calculated *in situ* R_{rs} spectra were plotted against wavelength (Fig. 2.3a). For algorithm development, 29 R_{rs} spectra were selected. Some of the sites were excluded after a visual examination of errors in the spectra. The observed errors in the measured spectra were possibly due to sun-glint contamination.

2.2.5.2 Conversion of *in situ* hyperspectral remote sensing reflectance to sensor-specific remote sensing reflectance

The measured *in situ* hyperspectral measurements were weighted with the relative spectral response function of each Micasense RedEdge band (MicaSense, Inc., WA) for obtaining remote sensing reflectance for Micasense RedEdge® as:

$$Rrs\ (MS) = \frac{\int_{\lambda i}^{\lambda j} S(\lambda) Rrs(\lambda)}{\int_{\lambda i}^{\lambda j} S(\lambda)} \quad (2.5)$$

where R_{rs} (MS) is the remote sensing reflectance computed for the Micasense RedEdge® spectral bands, R_{rs} is the hyperspectral remote sensing reflectance, λ_i and λ_j are the lower and upper limits of the bands, and S(λ) is the relative spectral response function of the Micasense RedEdge® spectral bands (Kidder and Vonder Haar 1995; Schowengerdt 2006). The calculated *in situ* R_{rs} spectra were plotted against wavelength and are shown in figure 2.3(b).

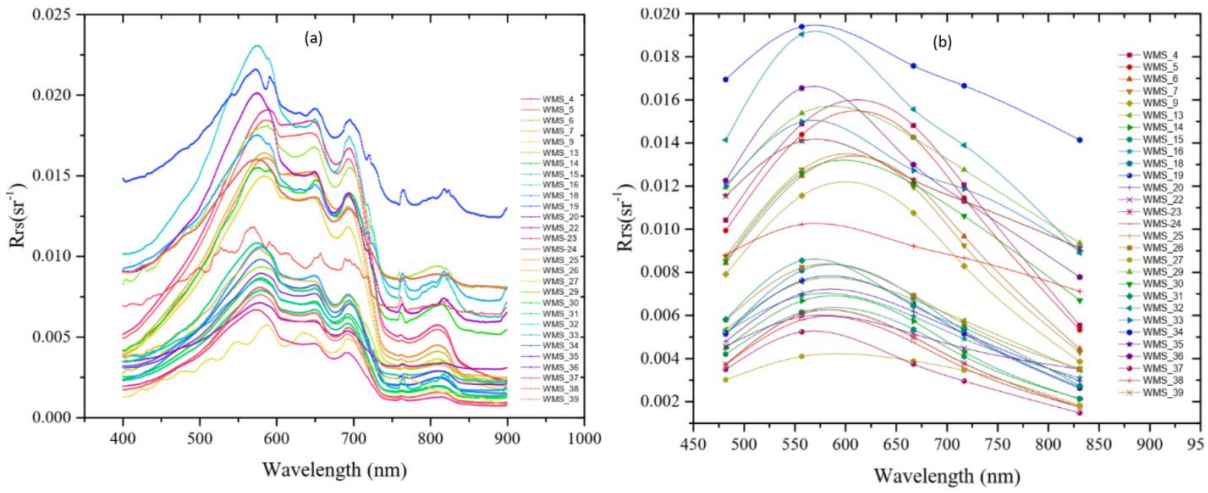

Figure 2.3 Variation of remote sensing reflectance spectra (a) measured by using GER-1500, (b) derived by Micasense RedEdge sensor.

2.2.6 R_{rs} model calibration and validation

Algorithms for estimating CDOM were calibrated using randomly selected 70% of the dataset (17 data points) and validated using the remaining 30% of the dataset (7 data points). Random sampling was performed using the SPSS ® software. A total of 15 published algorithms were tested using the dataset of this study and it was found that the algorithms reported by Koponen et al. (2007) for retrieving $a_{CDOM}(400)$ and the algorithms reported by Del Castillo & Miller (2008) and D'sa & Miller (2003) for retrieving $a_{CDOM}(412)$ yielded best estimates using hyperspectral data. In a similar manner, from a total of 10 published algorithms, the algorithm reported by Griffin et al. (2011) produced best estimates of $a_{CDOM}(400)$ with the dataset of this study for the RedEdge sensor. Following Koponen et al. (2007) R_{rs} at 663 and 490 nm were used for developing an algorithm for estimating $a_{CDOM}(400)$ while a combination of bands used by Del Castillo & Miller (2008) and D'sa & Miller (2003) including R_{rs} at 443, 510 and 670 nm were used for developing an algorithm for estimating $a_{CDOM}(412)$ using hyperspectral data. Similarly, a RedEdge algorithm was developed using RedEdge bands centered at 482 and 667 nm following Griffin et al. (2011) for estimating $a_{CDOM}(400)$. A modification of the functional form of these algorithms from linear to power-law produced better estimates. The coefficients were then optimized using Solver tool in Microsoft Excel to obtain best estimates. Calibration of each model was performed calculating the best fit functions based on least-squares regression analysis. The calibrated equations of a_{CDOM} were used to calculate the estimated a_{CDOM} for validation.Applicability and accuracy of the algorithms were determined by comparing the

estimated and the measured a_{CDOM} values. The comparison was expressed in terms of root mean squared error (RMSE), relative mean squared error (RMSE %), bias, and scatter index (S.I.) as:

$$RMSE = \sqrt{\frac{1}{N}\sum_{i=1}^{n}([Estimated - Measured]^2)} \quad (2.6)$$

$$Bias = \frac{\sum_{i=1}^{n}(Xi\ Estimated - Xi\ Measured\ )}{n} \quad (2.7)$$

$$Scatter\ Index = \frac{1}{X}\sqrt{\frac{1}{N}\sum_{i=1}^{n}([(yi - y\ ) - (Xi - X^{-})]^2)} \quad (2.8)$$

where n is the number of observations, while y_i is estimated, and x_i is the laboratory measured a_{CDOM} values.

2.3 Results and discussion

2.3.1 Discharge and biogeochemical parameters

During the sampling period, water level data for both Wolf River (WR) and Jourdan River (JR) showed a relatively high gauge height during March sampling period, 206.6 ± 3.7 cm and 29.6 ± 0.5 cm, respectively (Table 2.2; Figure 2.4). A noticeably higher (19.97 ± 13.30 m^3/s) and a lower (3.76 ± 3.18m^3/s) river discharge of WR was observed during March and May 2018, respectively (Table 2.2).

Table 2.2 Calculated average water level and discharge for the Wolf River and Jourdan River

Dates	Average Gauge Height (cm)		Average Discharge (m^3/s)	
	Wolf River	Jourdan River	Wolf River	Jourdan River
6-8, March 2018	206.6	29.6	19.97	n/a
7-12, May 2018	164.5	21.7	3.76	n/a
18-20,June 2018	172.9	39.3	4.60	n/a
16-20,July 2018	202.7	29.5	13.81	n/a

*Average gauge heights were calculated by considering the residence time of BSL
n/a refers to data not available
Source: https://waterdata.usgs.gov/nwis

Measured values of a_{CDOM} and DOC during spring and summer is given in Table 2.3. The measured salinity values vary from 3.9 psu to 20.1 psu showing a gradual increase from spring (March) to summer (May, June, and July), which corresponded well with observed river discharge. Further, measured absorption values of CDOM at 400 and 412 nm showed relatively higher absorption values in spring (0.0188 ± 0.0075 m^{-1} and 0.0140 ± 0.0056 m^{-1}) compared to values measured in summer period (0.0155 ± 0.0055 m^{-1} and 0.0140 ± 0.0053 m^{-1}). Similarly, measured DOC concentrations were higher in March (4.93 ± 0.16 mg/L) and lower in May (4.04 ± 2.04 mg/L) (Table 2.3). These observations indicate that the study area has a dynamic environmental setting and several factors may be responsible for regulating DOM fluxes. In particular, terrestrial freshwater inputs, mixing of solutes (Cai et al., 2012), and seasonal variations (Duan et al., 2007) can be the possible factors affecting DOM dynamics in WMS area. Previous studies reported that, during high discharge events, WR and JR bring significant amount of DOM to the study area (Wang et al., 2010). Further, Wang et al. (2010) reported that JR brings higher amounts of DOC and total dissolved carbohydrates (TCHO) compared WR. In addition to freshwater flows from both WR and JR, Mississippi sound receives freshwater input from many rivers along the Louisiana, Mississippi, and Alabama coasts, including Pearl River, Pascagoula River, Mobile, and also from the Mississippi River through the Bonnet Carre Spillway (Chigbu et al., 2004).

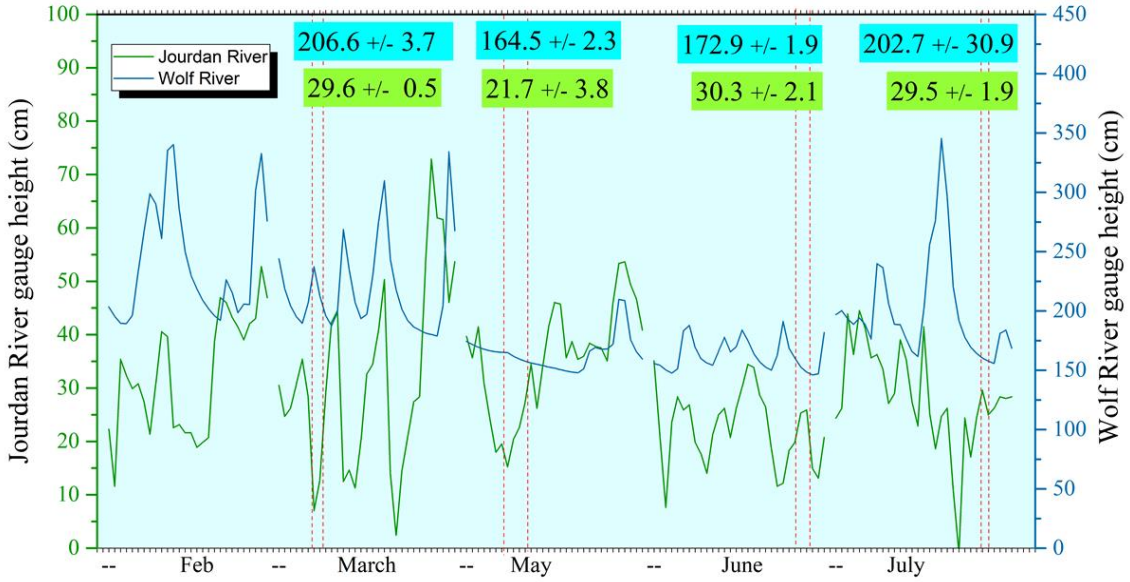

Figure 2.4 Time series of Jourdan River (green) and Wolf River (blue) gauge heights recorded by gauge station USGS 02481660 Jourdan River near Bay St Louis and USGS 02481510 Wolf River near Landon, MS

Table 2.3 Maximum, minimum, average, and standard deviation (s.d) of measured physicochemical parameters during spring and summer

	Spring				Summer			
	Salinity	a_{CDOM} (m^{-1})		**DOC***	**Salinity**	a_{CDOM} (m^{-1})		**DOC***
	(psu)	400	412	(mg/L)	(psu)	400	412	(mg/L)
Max.	20.1	0.0315	0.0287	4.38	6.61	0.0337	0.0315	5.06
Min.	7.67	0.0081	0.0066	3.73	3.9	0.0156	0.0127	4.59
Avg.	12.6	0.0155	0.0101	4.04	4.76	0.0188	0.014	4.93
s.d	3.78	0.0056	0.0053	2.04	1.1	0.0057	0.0059	0.16

*DOC measured for samples collected in March (spring) and May (summer).

2.3.2 Algorithms for estimating a_{CDOM}

2.3.2.1 Algorithm for the Nanohyperspec hyperspectral sensor

Remote sensing algorithms for estimating a_{CDOM} were derived by regression of above-water reflectance and a_{CDOM} measurements during the sampling period. Koponen et al. (2007) reported an algorithm for estimating a_{CDOM} in the Gulf of Finland by using a ratio of MEdium Resolution Imaging Spectrometer (MERIS) bands 3 and 7 centered at 490 and 663 nm. Application of this algorithm to the dataset of this study resulted in an R^2 of 0.52 when both spring and summer data was used (n=29), while an R^2 of 0.64 yielded when the data collected during the summer (n=24) was used (Table 2.4). Modifications to the functional form of the algorithm reported by Koponen et al. (2007) by introducing a power function to the band ratio and an additive term with the 663 nm band with a multiplicative coefficient for the independent variable and optimization of the coefficients yielded the following algorithm:

$$Y = 0.02724X - 0.02341 \quad (2.10)$$

where, Y= a_{CDOM} (400) and X= $\left(\frac{Rrs663}{Rrs490}\right)^{1.13} + 14.09(Rrs663)$

This modification to the functional form and optimization of the coefficients increased the R^2 to 0.75 (n=17) with an intercept of 0.02724, and a slope of 0.02341 (Table 2.5; Fig. 2.5 (a)). Match-up comparison between *in situ* measured a_{CDOM} (400) and algorithm estimated a_{CDOM} (400) with a subset of randomly selected samples (n=7) yielded an RMSE value of 0.026 m^{-1} (Table 2.5; Fig. 2.5 (b)). The algorithm was further assessed using a bias function and S.I.. and a bias of 0.0001 and S.I. of 0.168 were observed, which suggested the robustness of the algorithm in estimating a_{CDOM} at 400 nm (Table 2.5).

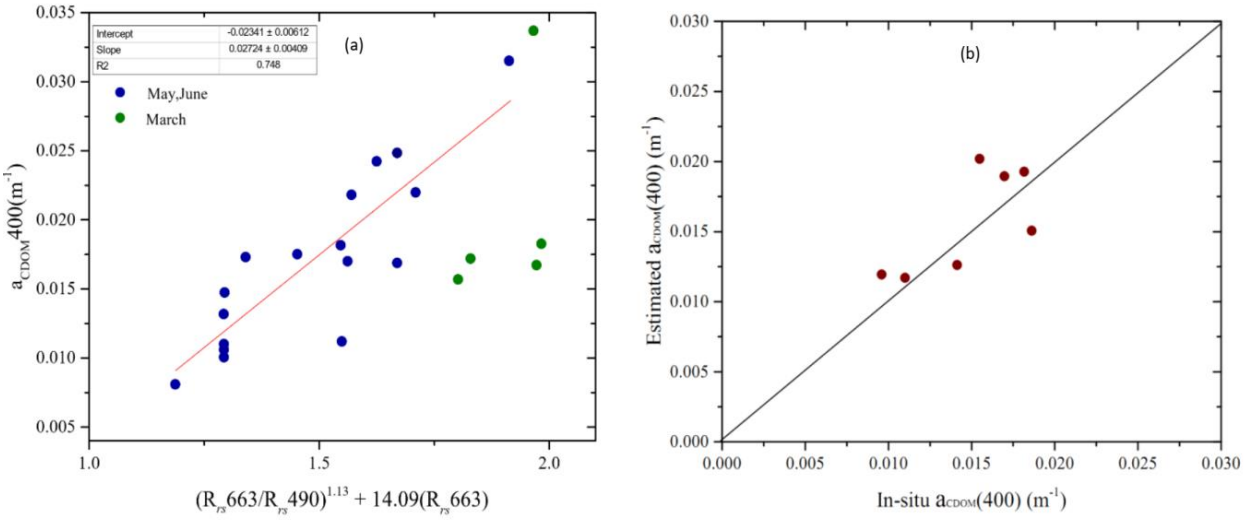

Figure 2.5 The algorithm developed using (a) a_{CDOM} (400) and *in situ* measured hyperspectral R_{rs} at 490, and 663 nm. (b) a_{CDOM} (400) estimated from algorithm 1 versus measured a_{CDOM} (400)

Del Castillo and Miller (2008) developed an algorithm for estimating a_{CDOM} (412) with R_{rs} at 510 nm and 670 nm of the Sea-Viewing Wide Field-of-View Sensor (SeaWiFS) while D'sa and Miller (2003) developed an algorithm with 443 nm and 510 nm bands of SeaWiFS. When these algorithms were tested with the combined dataset of spring and summer from this study, R^2 (n=29) of 0.44 and 0.28 were obtained for the algorithms reported by Del Castillo and Miller (2008) and D'sa and Miller (2003), respectively (Table 2.4). Use of only the summer dataset (n=24) yielded R^2 of 0.56 and 0.26 for the algorithms reported by Del Castillo and Miller (2007) and D'sa and Miller (2003), respectively (Table 2.4).

A 3-band algorithm was tested by combing the bands used in both these studies with a modified functional form as before by introducing a power function to the band ratio and an

additive term with the 663 nm band with a multiplicative coefficient and optimization of the coefficients yielded the following algorithm:

$$Y = 0.00236X + 0.00867 \quad (2.11)$$

where, $Y = aCDOM(412)$ *and* $X = \left(\frac{Rrs510}{Rrs670}\right)^{-4.7} + 1.82(Rrs443)$

The new relationship showed a statistically strong correlation with $R^2 = 0.70$ ($p<0.001$, n=17; Fig. 2.6a) and yielded an RMSE, bias, and S.I. of 0.0040 m^{-1}, 0.005 m^{-1}, 0.246 m^{-1} , respectively (Table 2.5; Fig. 2.6b). The observed results suggested that the modified Koponen et al. (2007) algorithm performed better in retrieving $a_{CDOM}(400)$ while the combined approach of Del Castillo and Miller (2008) and D'sa and Miller, (2003) performed well in retrieving $a_{CDOM}(412)$ in this study area. Majority of remote sensing algorithms used the short wavelength bands (e.g. blue or green bands) for estimating a_{CDOM} accurately (Pierson and Strömbeck, 2000; D'sa and Miller, 2003; Kallio et al., 2005; Kutser et al., 2005b; Koponen et al., 2007; Del Castillo and Miller, 2008; Mannino et al., 2008). Pierson and Strömbeck (2000) reported that bands between 412 – 560 nm could be used for a_{CDOM} estimation but use of bands close to 490 nm is advantageous because these bands are short enough to be strongly influenced by CDOM absorption, but they are a not in the shortest blue wavebands where atmospheric correction is particularly difficult. In this study, 443, 490, and 510 nm have been used, which produced reasonable estimates of a_{CDOM}. Recent studies showed that use of red band with another band in the visible range (e.g., blue) to estimate the CDOM for minimizing the interference effects of suspended particulates (Bowers et al., 2000, 2004). Kallio et al. (2005) developed a set of algorithms for estimating CDOM by using a ratio of

short wavelength bands (e.g. 450-520 nm) and long wavelength bands (e.g. 630-690 nm). Kallio et al. (2005) argued that

changes in R_{rs} due to CDOM absorption in the short wavelength region if normalized by changes in R_{rs} not related to CDOM in the longer wavelengths produces better estimation of CDOM. They claimed that 660-680 nm is the best region for normalization, and is probably due to the small variation in reflectance. In this study, 663 and 670 nm has been used for normalization, which improved the algorithms.

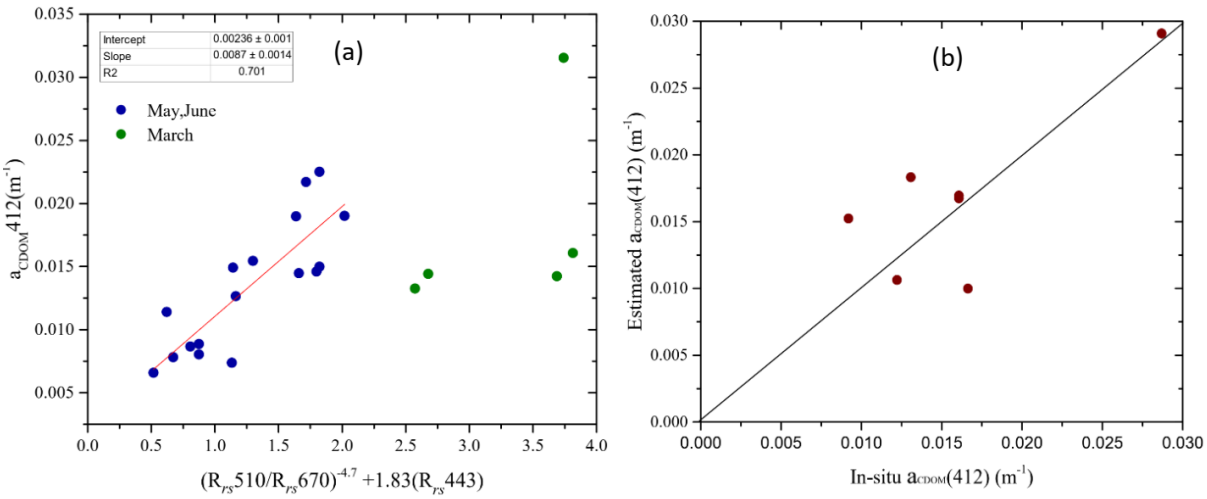

Figure 2.6 The algorithm developed using (a) a_{CDOM} (412) and *in situ* measured hyperspectral R_{rs} at 443,510, and 670 nm. (b) a_{CDOM} (412) estimated from algorithm 2 versus measured a_{CDOM} (412).

2.3.2.2 Algorithm for the Micasense RedEdge Multispectral sensor

In order to evaluate the functionality of the Micasense RedEdge Multispectral sensor, the third algorithm was developed by first computing to R_{rs} at each Micasence RedEdge bands by weighting *in situ* measured radiometer hyperspectral data with the relative spectral response

function of each Micasence RedEdge bands and then averaging (Fig. 2.3b). A number of previous studies have used the weighted and averaged R_{rs} by using the sensor's spectral response functions for remote sensing algorithm development (Martins et al., 2018; Hu et al., 2004; Kidder and Vonder Haar 1995, Schowengerdt 2006). Griffin et al. (2011) reported an algorithm for estimating a_{CDOM} by using bands centered at 485, 557, and 667 nm. Application of this algorithm to the dataset of this study resulted in an R^2 of 0.1 when both spring and summer data was used (n=29), while an R^2 of 0.05 yielded when the data collected during the summer (n=24) was used (Table 2.4). Modifications to the functional form of the algorithm reported by Griffin et al. (2011) by introducing a power function to the band ratio of RedEdge bands centered at 482 and 667 nm and optimization of the coefficients yielded the following algorithm:

$$Y = 0.00590X + 0.00284 \quad (2.13)$$

where, $Y = a_{CDOM}(412)$ and $X = \left(\frac{Rrs482}{Rrs667}\right)^{-5.78}$

This algorithm yielded an R^2 of 0.81 ($p<0.001$, n=17) between R_{rs} and $a_{CDOM}(412)$ (Fig.2.7a). Application of this algorithm to the validation dataset resulted in an RMSE of 0.0052 m^{-1} with a bias of 0.002 m^{-1}, and S.I. of 0.338 m^{-1} (Fig. 2.7b).

Griffin et al. (2011) used band ratios of blue, green, and red bands as dependent variables for algorithm development by using Landsat TM and ETM+. In the above algorithm, the blue band was used to retrieve CDOM while the red band was selected as the denominator in order to normalize the changes in R_{rs} not related to CDOM especially to avoid the contribution of chl-*a* from the optical signal (Pierson and Strömbeck, 2000; Kallio et al., 2005; Gitelson et al., 2008; Mishra and Mishra, 2012). Along the similar lines with the algorithms developed for the hyperspectral sensor, using both spring and summer data for the regression between $a_{CDOM}(412)$

and remotely sensed yielded an R^2 of 0.49 (n=29). However, use of summer data for algorithm development yielded an improved algorithm with an R^2 of 0.81.

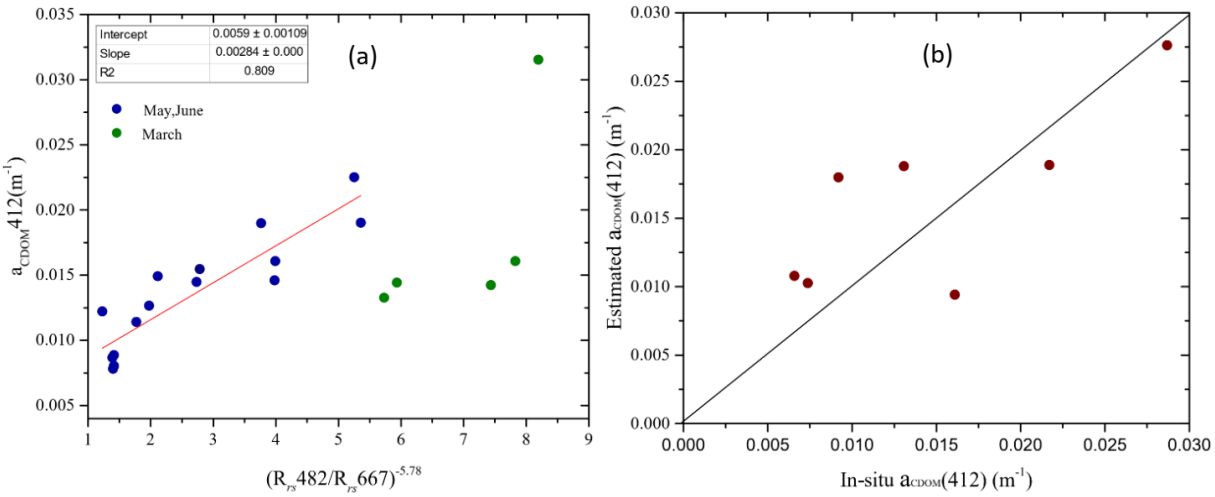

Figure 2.7 The algorithm developed using (a) a_{CDOM} (412) and *in situ* measured derived multispectral R_{rs} at 482 and 667 nm. (b) a_{CDOM} (412) estimated from algorithm 3 versus measured a_{CDOM} (412).

The 443, 482, and, 490 bands were chosen since they were at a short enough wavelength to be strongly influenced by the absorption of CDOM, but it was not in the shortest blue wavebands where atmospheric correction is particularly difficult (Pierson and Strömbeck 2000). Especially, atmospheric interference is high at 412 nm band and it was not selected for algorithm development in this study (Barnard et al., 1998; Siegel et al., 2000).

510 nm and 670 nm used as a good index of CDOM abundance in the river plume because, in low-salinity river plume waters, most of the light attenuation is controlled by CDOM (Del Castillo et al., 1999; D'Sa & Miller, 2003; D'Sa et al., 2006). Tehrani et al. (2013) reported that R_{rs}(510) could be utilized for CDOM algorithms which is sensitive to CDOM optical signatures in

surface waters. Even though CDOM does not absorb strongly at the red band (663 nm), 660-680 nm region considers as the best region for normalizing and is probably due to its small variation in reflectance (Kallio et al., 2005). Hence, CDOM absorption in the short wavelength region is normalized by changes in reflection not related to CDOM in the longer wavelengths (Kallio et al., 2005; Slonecker et al., 2016)

Generally, the band ratio is commonplace throughout the remote sensing community (Attila et al., 2012). Typically, a minimum of one simple band ratio is sufficient for developing the empirical algorithms used to obtain coefficients with R_{rs} and measured CDOM. As an example, Zhu et al. (2014) analyzed fifteen algorithms for retrieving CDOM; the results showed that accuracy of estimated CDOM is low when simple band ratios with wavelengths lower than 550 nm are used. Hence, in this study, at least one higher wavelength band has been used in order to obtain higher accuracy. This study shows the applicability of hyperspectral and multispectral R_{rs} data for estimating a_{CDOM} using UAS data.

Absorption of CDOM in NGoM region is highly responsive to the seasonal variations as reported in previous studies (Cai et al., 2011; Tehrani et al., 2013), which was observed in this study as well. When both spring and summer data were used an R^2 of 0.52 was obtained with the Koponen et al. (2007) approach and an R^2 of 0.44 was obtained with the combined approach of Del Castillo and Miller (2008) and D'sa and Miller, (2003). Figure 2.8 shows the *in situ* measured a_{CDOM} *versus* salinity. Samples collected during May and June showed a decreasing conservative mixing of a_{CDOM} while the discharge was low. Samples collected in March showed an increasingconservative mixingduring while the discharge was high (Fig. 2.8). Similarly, previous studies also reported that seasonal variability affects the hydrographic and bio-optical properties

in the NGoM region significantly (D'sa and Miller, 2003). In order to account for the sensitivity of a_{CDOM} to seasonal variations, the algorithms were developed by considering seasonality. Because of the seasonality, samples collected during the summer were used with the measured R_{rs} to yield robust algorithms.

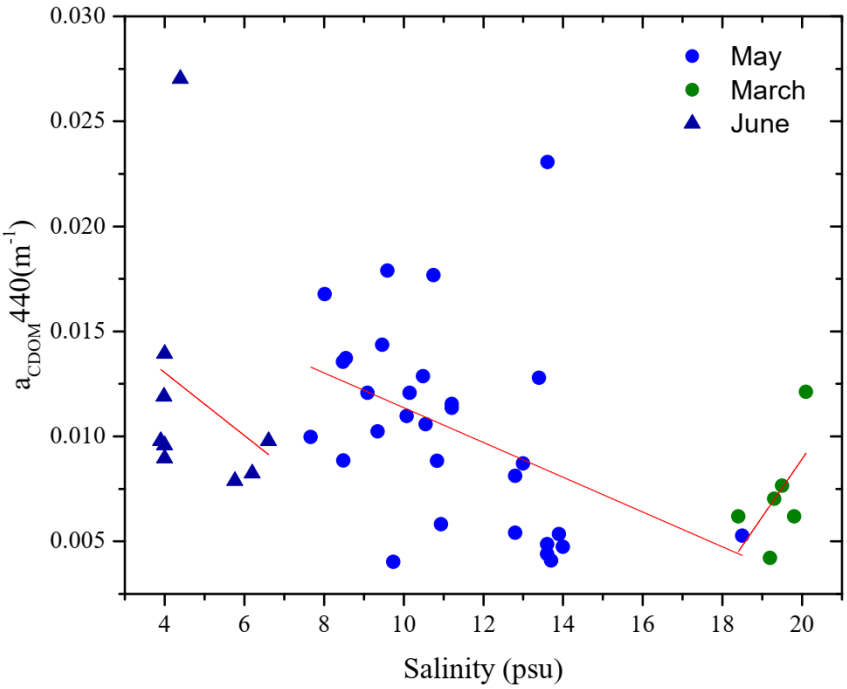

Figure 2.8 Measured a_{CDOM} (412) values versus salinity.

Figure 2.9 shows the measured absorption coefficient spectra of CDOM, where a higher CDOM absorption was observed around band 1 (blue, 475 ± 20 nm) and band 2 (green, 560 ± 20 nm) region and the absorption continually drops for longer wavelengths. Further, in band 4 (red, 668 ± 10 nm) and band 5 (NIR, 840 ± 40 nm) there was minimal influence of CDOM. Hence, in the algorithms developed in this study, short wavelengths were used for CDOM algorithm

devel;opment and long wavelengths were used to normalize the effect of other optically active constituents. Kutser et al. (2005b) indicated that the longer wavelength bands for Landsat, IKONOS, and Advanced Land Imager (ALI) (630-690 nm) are not sensitive to CDOM and used them to normalize the effect of other optically active constituents.

Table 2.4 Comparison of R^2 of previously reported algorithms with R^2 obtained after modification of algorithm coefficients using the data from this study.

Study	Functional Form	X	Y	R^2		
				reported*	Spring & summer**	Summer***
Koponen et al.(2007)	Y=4.41X-0.52	$R_{rs}(663)/ R_{rs}(490)$	a_{CDOM} (400)	0.98 (n=9)	0.52 (n=29)	0.64 (n=24)
Del Castillo and Miller, (2008)	Y=-0.90 X+2.34	$R_{rs}(510)/ R_{rs}(670)$	a_{CDOM} (412)	0.94 (n=10)	0.44 (n=29)	0.56 (n=24)
D'sa and Miller (2003)	Y=-0.9874-2.025logX	Rrs(443)/ $R_{rs}(510)$	log(a_{CDOM} (412))	0.86 (n=19)	0.28 (n=29)	0.26 (n=24)
Griffin et al. (2011)	$Y=1.45+26.529(X_1)+0.603(X_2)$	$X_1= R_{rs}(667)$	ln(a_{CDOM} (400))	0.78 (n=59)	0.10 (n=29)	0.05 (n=24)
		$X_2 = R_{rs}(557)/R_{rs}(485)$				

* R^2 reported by authors
** R^2 obtained when fitted with the data collected during both spring and summer in this study
*** R^2 obtained when fitted with the data collected during summer in this study

Table 2.5 Algorithm R^2 after modifying the functional form and the coefficients using randomly selected 70% of the summer dataset for algorithm calibration and root mean squared error (RMSE), bias, and scatter index (SI) using remaining 30% of the data for algorithm validation.

Algorithm	Functional Form	X	Y	Summer R^2 (n=17)	RMSE (m^{-1}) (n=7)	Bias (n=7)	S.I. (n=7)
1	$Y=X_1^a + b(X_2)$	$X_1=R_{rs}(663)/ R_{rs}(490)$	a_{CDOM} (400)	0.75 (a=1.13, b=14.09)	0.0026	0.0001	0.168
2	$Y=X_1^a + b(X_2)$	$X_2= R_{rs}(663)$ $X_1= R_{rs}(510)/ R_{rs}(670)$ $X_2= R_{rs}(443)$	a_{CDOM} (412)	0.70 (a= -4.7, b=1.8205)	0.0040	0.0050	0.246
3	$Y=X_1^a$	$X_1= R_{rs}(482)/ R_{rs}(667)$	a_{CDOM} (412)	0.81 (a=-5.78)	0.0052	0.0020	0.338

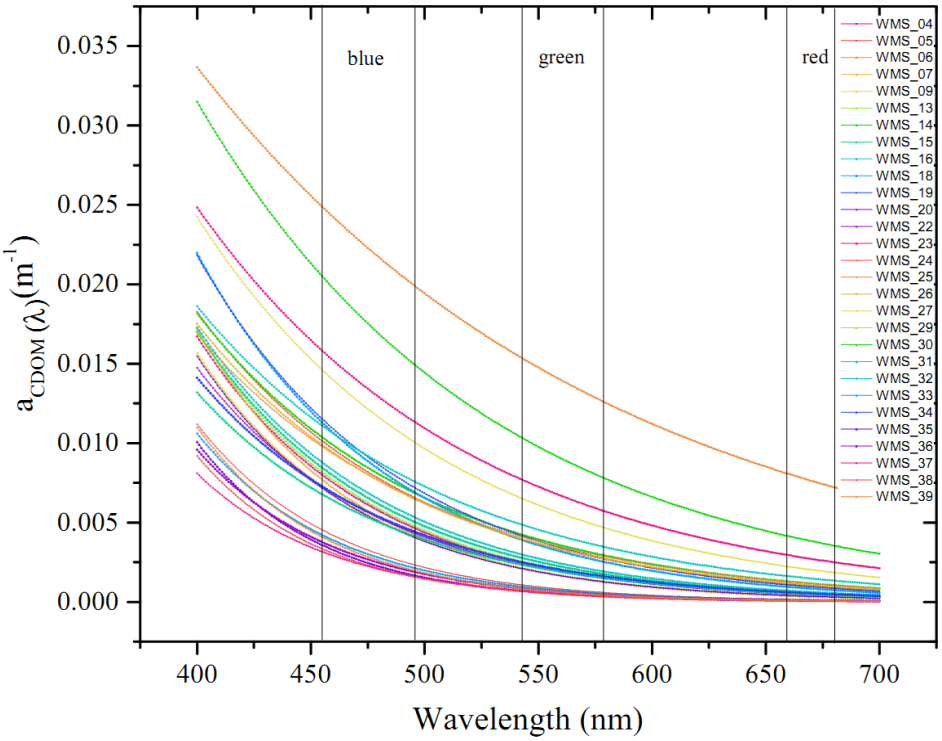

Figure 2.9 The exponential decrease nature of absorption of CDOM with respect to wavelengths in the electromagnetic spectrum and distribution of blue, green, and red bands of Micasense RedEdge® sensor.

2.4 Conclusions

Remote sensing algorithms were developed using hyperspectral and multispectral surface water reflectance data for estimating CDOM. Three successful algorithms were developed by selecting R_{rs} at 482, 490, 520, 663, and 670 nm bands. With the Nano-hyperspec hyperspectral data, two band ratio algorithms were developed, which yielded R^2 of 0.75 and 0.70 for estimating $a_{CDOM}(400)$ and $a_{CDOM}(412)$, respectively. The algorithm developed for the RedEdge multispectral sensor yielded an R^2 of 0.81 for estimating $a_{CDOM}(412)$.Validation results of algorithms show the successful retrieval of a_{CDOM} with multispectral and hyperspectral sensors

with RMSE (0.0026 m^{-1}, 0.0040 m^{-1}, and 0.0052 m^{-1}) and bias (0.0001 m^{-1}, 0.0050 $m^{-1,}$ and 0.0020 m^{-1}). Accuracies of these algorithms increased when the seasonal variability was accounted for. For band ratio algorithms, shorter wavelength bands (443, 482,490, & 510 nm) were found as optimal for estimation of a_{CDOM} while longer wavelength bands (663, 670, & 667 nm) were found as optimal for normalization of the signal other than a_{CDOM} in coastal waters.

These hyperspectral and multispectral algorithms for a_{CDOM} can be used to track the inputs of terrigenous organic matter from rivers or estuaries into the coastal ocean. In order to protect the commercially and ecologically important oyster beds located in the Henderson Point and Pass Christian, estimation of CDOM and evaluation of DOM will help narrow down the possible anthropogenic and natural impacts on the oyster reefs of western Mississippi Sound. This study provides an approach for estimation of a_{CDOM} with UAS imagery that can be applied to develop time-series of images CDOM for water quality management purposes in western Mississippi Sound as well as other regions around the globe.

2.5 REFERENCES

Alesheikh, A.A., Ghorbanali, A. and Nouri, N., 2007. Coastline change detection using remote sensing. *International Journal of Environmental Science & Technology*, *4*(1), pp.61-66.

Attila, J., Koponen, S., Kallio, K., Lindfors, A., Kaitala, S. and Ylöstalo, P., 2013. MERIS Case II water processor comparison on coastal sites of the northern Baltic Sea. Remote Sensing of Environment, 128, pp.138-149.

Barnard, A.H., Zaneveld, J.R.V., Pegau, W.S., Mueller, J.L. and Trees, C.C., 1998. SeaWiFS ocean color in the Gulf of California: Validation. In Ocean Optics XIV.

Bauer, J.E., Cai, W.J., Raymond, P.A., Bianchi, T.S., Hopkinson, C.S. and Regnier, P.A., 2013. The changing carbon cycle of the coastal ocean. Nature, 504(7478), p.61.

Beck, M.W., Brumbaugh, R.D., Airoldi, L., Carranza, A., Coen, L.D., Crawford, C., Defeo, O., Edgar, G.J., Hancock, B., Kay, M.C. and Lenihan, H.S., 2011. Oyster reefs at risk and recommendations for conservation, restoration, and management. Bioscience, 61(2), pp.107-116.

Bhardwaj, A., Sam, L., Martín-Torres, F.J. and Kumar, R., 2016. UAVs as remote sensing platform in glaciology: Present applications and future prospects. Remote sensing of environment, 175, pp.196-204.

Blough, N.V., Del Vecchio, R., Hansell, D.A. and Carlson, C.A., 2002. Distribution and dynamics of chromophoric dissolved organic matter (CDOM) in the coastal environment. Biogeochemistry of Marine Dissolved Organic Matter.

Bukata, R.P., Jerome, J.H., Kondratyev, A.S. and Pozdnyakov, D.V., 1995. Optical properties and remote sensing of inland and coastal waters. CRC press.

Cai, Y., Guo, L., Wang, X., Mojzis, A.K. and Redalje, D.G., 2012. The source and distribution of dissolved and particulate organic matter in the Bay of St. Louis, northern Gulf of Mexico. Estuarine, Coastal and Shelf Science, 96, pp.96-104.

Carlson, C.A., Ducklow, H.W. and Michaels, A.F., 1994. Annual flux of dissolved organic carbon from the euphotic zone in the northwestern Sargasso Sea. Nature, 371(6496), p.405.

Chigbu, P., Gordon, S. and Strange, T., 2004. Influence of inter-annual variations in climatic factors on fecal coliform levels in Mississippi Sound. Water Research, 38(20), pp.4341-4352.

Chen, R.F. and Gardner, G.B., 2004. High-resolution measurements of chromophoric dissolved organic matter in the Mississippi and Atchafalaya River plume regions. Marine Chemistry, 89(1-4), pp.103-125.

Del Castillo, C.E., Coble, P.G., Morell, J.M., Lopez, J.M. and Corredor, J.E., 1999. Analysis of the optical properties of the Orinoco River plume by absorption and fluorescence spectroscopy. Marine Chemistry, 66(1-2), pp.35-51.

Del Castillo, C.E. and Miller, R.L., 2008. On the use of ocean color remote sensing to measure the transport of dissolved organic carbon by the Mississippi River Plume. Remote Sensing of Environment, 112(3), pp.836-844.

D'Sa, E.J. and Miller, R.L., 2003. Bio-optical properties in waters influenced by the Mississippi River during low flow conditions. Remote sensing of environment, 84(4), pp.538-549.

D'sa, E.J., Miller, R.L. and Del Castillo, C., 2006. Bio-optical properties and ocean color algorithms for coastal waters influenced by the Mississippi River during a cold front. Applied Optics, 45(28), pp.7410-7428.

Duan, S., Bianchi, T.S. and Sampere, T.P., 2007. Temporal variability in the composition and abundance of terrestrially-derived dissolved organic matter in the lower Mississippi and Pearl Rivers. Marine Chemistry, 103(1-2), pp.172-184.

Gray, J.S., Wu, R.S.S. and Or, Y.Y., 2002. Effects of hypoxia and organic enrichment on the coastal marine environment. Marine ecology progress series, 238, pp.249-279.

Griffin, C.G., Frey, K.E., Rogan, J. and Holmes, R.M., 2011. Spatial and interannual variability of dissolved organic matter in the Kolyma River, East Siberia, observed using satellite imagery. Journal of geophysical research: Biogeosciences, 116(G3).

Gitelson, A.A., Dall'Olmo, G., Moses, W., Rundquist, D.C., Barrow, T., Fisher, T.R., Gurlin, D. and Holz, J., 2008. A simple semi-analytical model for remote estimation of chlorophyll-a in turbid waters: Validation. Remote Sensing of Environment, 112(9), pp.3582-3593.

Herbland, A., Le Bouteiller, A. and Raimbault, P., 1985. Size structure of phytoplankton biomass in the equatorial Atlantic Ocean. Deep Sea Research Part A. Oceanographic Research Papers, 32(7), pp.819-836.

Ho, P., Shim, M.J., Howden, S.D. and Shiller, A.M., 2019. Temporal and spatial distributions of nutrients and trace elements (Ba, Cs, Cr, Fe, Mn, Mo, U, V, and Re) in Mississippi coastal waters: Influence of hypoxia, submarine groundwater discharge, and episodic events. Continental Shelf Research, 175, pp.53-69.

Hu, C., Muller-Karger, F.E. and Zepp, R.G., 2002. Absorbance, absorption coefficient, and apparent quantum yield: A comment on common ambiguity in the use of these optical concepts. Limnology and Oceanography, 47(4), pp.1261-1267.

Jaffé, R., Boyer, J.N., Lu, X., Maie, N., Yang, C., Scully, N.M. and Mock, S., 2004. Source characterization of dissolved organic matter in a subtropical mangrove-dominated estuary by fluorescence analysis. Marine Chemistry, 84(3-4), pp.195-210.

Kallio, K., Pulliainen, J. and Ylöstalo, P., 2005. MERIS, MODIS and ETM+ channel configurations in the estimation of lake water quality from subsurface reflectance using semianalytical and empirical algorithms. Geophysica, 41(1-2), pp.31-55.

Koponen, S., Attila, J., Pulliainen, J., Kallio, K., Pyhälahti, T., Lindfors, A., Rasmus, K. and Hallikainen, M., 2007. A case study of airborne and satellite remote sensing of a spring bloom event in the Gulf of Finland. Continental Shelf Research, 27(2), pp.228-244.

Kutser, T., Pierson, D.C., Tranvik, L., Reinart, A., Sobek, S. and Kallio, K., 2005b. Using satellite remote sensing to estimate the colored dissolved organic matter absorption coefficient in lakes. Ecosystems, 8(6), pp.709-720.

Kutser, T., Verpoorter, C., Paavel, B. and Tranvik, L.J., 2015. Estimating lake carbon fractions from remote sensing data. Remote Sensing of Environment, 157, pp.138-146.

Kidder, S.Q. and Haar, T.V., Satellite Meteorology: An Introduction. 1995.

Laanen, M.L., 2007. Yellow matters: improving the remote sensing of coloured dissolved organic matter in inland freshwaters.

La Peyre, M.K., Nix, A., Laborde, L. and Piazza, B.P., 2012. Gauging state-level and user group views of oyster reef restoration activities in the northern Gulf of Mexico. Ocean & coastal management, 67, pp.1-8.

Lee, Z., Carder, K.L., Mobley, C.D., Steward, R.G. and Patch, J.S., 1999. Hyperspectral remote sensing for shallow waters: 2. Deriving bottom depths and water properties by optimization. Applied optics, 38(18), pp.3831-3843.

Lipovsky, V.P. and Chew, K.K., 1972. Mortality of Pacific Oysters (Crassotrea Gi-Gas): The Influence of Temperature and Enriched Seawater on Oyster Survival.

Malham, S.K., Cotter, E., O'Keeffe, S., Lynch, S., Culloty, S.C., King, J.W., Latchford, J.W. and Beaumont, A.R., 2009. Summer mortality of the Pacific oyster, Crassostrea gigas, in the Irish Sea: the influence of temperature and nutrients on health and survival. Aquaculture, 287(1-2), pp.128-138.

Mannino, A., Russ, M.E. and Hooker, S.B., 2008. Algorithm development and validation for satellite-derived distributions of DOC and CDOM in the US Middle Atlantic Bight. Journal of Geophysical Research: Oceans, 113(C7).

Martins, S., Chokmani, K., Alcântara, E., Ogashawara, I. and El-Alem, A., 2018. Mapping the coloured dissolved organic matter absorption coefficient in a eutrophic reservoir using remotely sensed images. Inland Waters, 8(4), pp.488-504.

McCarthy, M.J., Varty, K., Naylor, A.R., London, N.J.M. and Bell, P.R.F., 1998. Bilateral infrainguinal vein grafts and the incidence of vein graft stenosis. European journal of vascular and endovascular surgery, 15(3), pp.231-234.

Mishra, S. and Mishra, D.R., 2012. Normalized difference chlorophyll index: A novel model for remote estimation of chlorophyll-a concentration in turbid productive waters. Remote Sensing of Environment, 117, pp.394-406.

Mobley, C.D., 1999. Estimation of the remote-sensing reflectance from above-surface measurements. Applied optics, 38(36), pp.7442-7455.

Mobley, C.D., 2004. Optical modeling of ocean waters: Is the case 1-case 2 classification still useful?. Oceanogr, 17(2), pp.60-67.

Nebiker, S., Annen, A., Scherrer, M. and Oesch, D., 2008. A light-weight multispectral sensor for micro UAV—Opportunities for very high resolution airborne remote sensing. The international archives of the photogrammetry, remote sensing and spatial information sciences, 37(B1), pp.1193-1199.

Ozesmi, S.L. and Bauer, M.E., 2002. Satellite remote sensing of wetlands. Wetlands ecology and management, 10(5), pp.381-402.

Prairie, Y.T., 2008. Carbocentric limnology: looking back, looking forward. Canadian Journal of Fisheries and Aquatic Sciences, 65(3), pp.543-548.

Pierson, D.C. and Strömbeck, N., 2000. A modelling approach to evaluate preliminary remote sensing algorithms: Use of water quality data from Swedish Great Lakes. Geophysica, 36(1-2), pp.177-202.

Pollack, J.B., Kim, H.C., Morgan, E.K. and Montagna, P.A., 2011. Role of flood disturbance in natural oyster (Crassostrea virginica) population maintenance in an estuary in South Texas, USA. Estuaries and Coasts, 34(1), pp.187-197.

Sawant, P.A., 2009. Factors influencing the environmental quality of the Bay of Saint Louis, Mississippi and implications for evolving coastal management policies.

Schowengerdt, R.A., 2006. Remote sensing: models and methods for image processing. Elsevier.

Siegel, D.A., Wang, M., Maritorena, S. and Robinson, W., 2000. Atmospheric correction of satellite ocean color imagery: the black pixel assumption. Applied optics, 39(21), pp.3582-3591.

Slonecker, E.T., Jones, D.K. and Pellerin, B.A., 2016. The new Landsat 8 potential for remote sensing of colored dissolved organic matter (CDOM). Marine pollution bulletin, 107(2), pp.518-527.

Smith, R.C. and Baker, K.S., 1978. The bio-optical state of ocean waters and remote sensing 1. Limnology and Oceanography, 23(2), pp.247-259.

Soletchnik, P., Faury, N., Razet, D. and Goulletquer, P., 1998. Hydrobiology of the Marennes-Oléron Bay. Seasonal indices and analysis of trends from 1978 to 1995. Hydrobiologia, 386(1-3), pp.131-146.

Soletchnik, P., Ropert, M., Mazurié, J., Fleury, P.G. and Le Coz, F., 2007. Relationships between oyster mortality patterns and environmental data from monitoring databases along the coasts of France. Aquaculture, 271(1-4), pp.384-400.

Solis, R.S., 1999. Hydrography, mixing characteristics, and residence times of Gulf of Mexico estuaries. Biogeochemistry of Gulf of Mexico estuaries.

Tehrani, N., D'Sa, E., Osburn, C., Bianchi, T. and Schaeffer, B., 2013. Chromophoric dissolved organic matter and dissolved organic carbon from sea-viewing wide field-of-view sensor (SeaWiFS), moderate resolution imaging spectroradiometer (MODIS) and MERIS sensors: Case study for the northern Gulf of Mexico. Remote Sensing, 5(3), pp.1439-1464.

Wang, X., Cai, Y. and Guo, L., 2010. Preferential removal of dissolved carbohydrates during estuarine mixing in the Bay of Saint Louis in the northern Gulf of Mexico. Marine Chemistry, 119(1-4), pp.130-138.

Werdell, P.J., Franz, B.A., Bailey, S.W., Feldman, G.C., Boss, E., Brando, V.E., Dowell, M., Hirata, T., Lavender, S.J., Lee, Z. and Loisel, H., 2013. Generalized ocean color inversion model for retrieving marine inherent optical properties. Applied optics, 52(10), pp.2019-2037.

Woodruff, D.L., Stumpf, R.P., Scope, J.A. and Paerl, H.W., 1999. Remote estimation of water clarity in optically complex estuarine waters. Remote Sensing of Environment, 68(1), pp.41-52.

Zhu, W., Yu, Q., Tian, Y.Q., Chen, R.F. and Gardner, G.B., 2011. Estimation of chromophoric dissolved organic matter in the Mississippi and Atchafalaya river plume regions using above-surface hyperspectral remote sensing. Journal of Geophysical Research: Oceans, 116(C2).

Zhu, W., Yu, Q., Tian, Y.Q., Becker, B.L., Zheng, T. and Carrick, H.J., 2014. An assessment of remote sensing algorithms for colored dissolved organic matter in complex freshwater environments. Remote Sensing of Environment, 140, pp.766-778.

CHAPTER III

PHYSICOCHEMICAL AND BIOGEOCHEMICAL FACTORS AFFECTING THE WATER QUALITY OF PASS CHRISTIAN AND HENDERSON OYSTER REEFS

3.1.1 Introduction

Dissolved organic matter (DOM) is one of the largest carbon reservoirs in the coastal ocean (Benner et al., 1992) and the most active and mobile fraction of the organic matter in nature (Bolan et al., 2011). Accordingly, DOM influences a spectrum of biogeochemical activities in aquatic environments (Bolan et al., 2011). Excessive DOM in coastal waters can cause serious environmental problems such as hypoxic conditions (Hetland and DiMarco, 2008), ocean acidification (Benner et al., 2002), harmful algal blooms (Heisler et al., 2008), and a reduction in light penetration (D'sa and DiMarco, 2009). DOM can also facilitate transportation of toxic elements and heavy metals (Stanley et al., 2012). Consequently, monitoring and management of DOM dynamics in coastal waters is important (Hansell et al., 2009). For effective management of DOM, it is essential to understand the sources, transportation processes, and fate of DOM in coastal waters and to determine the physical and biogeochemical processes controlling DOM both in the watershed and the waterbody.

Organic matter (OM) in aquatic systems occur either as dissolved organic matter (DOM) or particulate organic matter (POM) (Mostofa et al., 2013). DOM is composed of primarily dissolved organic carbon (DOC), dissolved organic nitrogen (DON), dissolved organic phosphorous (DOP), and dissolved organic sulphur (DOS), with DOC as the major component.

DOM can originate from land and transported through hydrological systems to aquatic environments, which is termed as allochthonous DOM. DOM that is produced *in situ* from the microbial decomposition of OM produced by phytoplankton are called autochthonous DOM (Hudson et al., 2007; Helms et al., 2008). The allocthonous fraction of DOM reaches the waterbodies predominantly from leaching of degraded terrestrial organic material. The main controls of allochthonous DOM are hydrology and land-use and land cover of the surrounding area (Mattson et al., 2009; Kalbitz et al., 2000; Sinsabaugh and Foreman, 2003). Both allochthonous and autochthonous DOM can undergo microbial degradation or abiotic processes such as photochemical degradation (Wershaw, 2004; Williams et al., 2010).

Terrestrially derived DOM is transported by streams and rivers to coastal waters (Schlesinger and Melack, 1981). Small streams entering the rivers add locally produced DOM (Schlesinger and Melack, 1981). Additionally, wetland discharge also brings in a substantial amount of DOM to the coastal waters (Bilby and Likens, 1979; Hedges, 1992). An estimated 0.25 x 10^{15} g of dissolved organic carbon (DOC) is transported into oceans annually as a result of terrestrial runoff (Maybeck, 1982). Winds and tidal actions also transport DOM in coastal waters, sometimes resuspending the bottom sediments and organic matter (Chen and Gardner, 2004; Hansell and Carlson, 2014). Other than surface runoff, at some locations subsurface groundwater discharge transports DOM to coastal waters (Santos et al., 2009). Thus, coastal waters are enriched with organic matter derived from both terrestrial and *in situ* sources (Benner and Opsahl, 2001; Dagg et al., 2004; Guo et al., 2009).

DOM in natural waters undergoes various biotic and abiotic processes that create different types of DOM by-products (Lin, 2015). For example, terrestrially derived complex DOM as well as in situ produced labile DOM undergo sunlight-induced decomposition (photodegradation) and

microbial degradation (biodegradation) resulting in much simpler DOM forms (Moran et al., 2000; Sankar et al., 2019). Apart from photo-biodegradation of DOM, flocculation processes transform DOM compounds in water bodies, especially at the freshwater and seawater salinity gradients (Benner and Opsahl, 2001). Further, transformation and reprocessing (removal) of DOM in water actively are linked to numerous processes such as microbial metabolism, nutrient uptake, the balance between autotrophy and heterotrophy, acidity, bioavailability, and release and binding of trace metals and contaminants, photochemical release of biologically labile organic compounds, photoproduction of trace gases, and phytoplankton activities (Benner, 2002; Stanley et al., 2012).

Numerous physical and biogeochemical parameters can regulate the quality and quantity of DOM, especially in coastal environments. Freshwater discharge carry a significant amount of DOM to coastal waters with high flow events transporting highest amount of DOM (Orlando et al., 1993; Wang et al., 2010; Cai et al., 2012). Salinity variation caused by mixing of fresh water with saline water transforms DOM in coastal environments. As a result of salinity variation, the distribution of DOM varies horizontally and vertically within the water column (Cai et al., 2012; Miller et al., 1998; Keith et al., 2015). Solar insolation alter the DOM composition through photochemical reactions (Blough and Del Vecchio 2002). DOM can interact with sunlight and, produce various types of photochemical by-products through photo-oxidation and photobleaching reactions (Krik, 1988; Voldacek et al., 1997). Temperature affects microbial activity in the water column. Lower intensity of solar energy together with lower temperatures results in reduced photosynthesis and as a result of reduced photosynthetic activities, microbial respiration rates can exceed the photosynthesis rates in the water column. Higher DOM concentrations can also limit light penetration reducing photosynthesis rates and increasing microbial respiration. Increased

microbial activity can affect coastal water pH levels (Cia et al., 2012). Lower pH levels are observed due to increasing of dissolved CO_2 levels by microbial respiration.

Increased microbial respiration also causes hypoxia, especially in the bottom waters. Bottom microbial communities can rapidly interact with the sunk organic matter by increasing rates of respiration, and carbon assimilation with a high DO demand (Moodley et al., 2002; Witte et al., 2003). As a result of such process, depleted oxygen conditions can be observed in coastal waters. Especially, density stratification caused by freshwater inputs and lower oxygen exchange between near-bottom water and the atmosphere causes hypoxic events. Hypoxic conditions in the northern Gulf of Mexico (NGoM) region has been reported since 1970s (Rabalais and Turner, 2001). Recent studies reported a progressive increment in the area of the hypoxic zone in the NGoM region (Obenour et al., 2013; Rabalais et al., 2002). For example, the average areal extent of 8000-9000 km^2 observed in mid-summer1985-1992 where increased hypoxic zone of 12,500 km^2 in mid-summer 1998 and area of 16,000- 20,700 km^2 found during 1993 to 2001 (Rabalais et al. 2002; Rabalais and Turner, 2001). Oyster diebacks happened as a result of hypoxia caused by excessive organic matter input to Western Mississippi Sound in summer 2017 (personal communication, Mississippi Department of Marine Resources).

Trace metals show a strong affinity to DOM, and as a result, they could potentially enhance the bio-accumulation of trace metals in benthic organisms (Guo et al., 2000; Haitzer et al., 1998; Wang et al., 2000). Urbanization and population growth in the gulf coast affect the water quality of the Bay St. Louis (Cai et al., 2012; Mojzis, 2010). Previous studies detailed the effects of water quality in NGoM due to nutrients and OM (Wang et al., 2010; Cai et al., 2012). However, the impact of water quality due to DOM dynamics in western Mississippi Sound region, especially over the oyster reefs is not well studied. Therefore, the main aim of this study was to assess the

effects of physical and biogeochemical factors on DOM dynamics over the Pass Christian and Henderson point oyster reefs in the western Mississippi Sound.

3.2 Methods and materials

3.2.1 Study area

3.2.1.1 Freshwater inputs

Coastal waters over the Henderson Point and Pass Christian reefs located in the western Mississippi Sound (WMS) southeast of Bay St. Louis (BSL) was considered as the study area for this research (Fig. 2.1). The depth around these reefs ranges from 1.0-3.5 m. Northern part of the area is connected to BSL estuary with a narrow pass of 3 km and the southern part is often exposed to WMS. Main freshwater flow comes from the BSL shallow micro-tidal drowned river valley (Eleuterius and Criss 1994). Jordan River (JR) and Wolf River (WR) are the primary freshwater sources to BSL and the study area. Annual fresh water discharge from WR ranges between <10 – 170 m^3/s (Lin et al., 2012). In addition to JR and WR, Bayou Prortage, located in the southern part of BSL, drains some freshwater to BSL. The mouth of this bayou provides access to the industrial park in West Harrison County (Eleuterius and Criss 1994). Apart from bayou Prortage, there are approximately 27 relativelely smaller bayous that drain into the BSL (GCRL 1978); the major ones are Catfish, Cutoff, Bayou LaCroix, Edwards, Watts, and Joe's on the western side, and Cedar, DeLisle, Bayou Acadian, Johnson, Mallini, and BP on the eastern side (Mojzis, 2010). Additionally, Mississippi Sound receives fresh water from the Pascagoula River and Mobile Bay outflow, which drains to the central and eastern Mississippi Sound and less significant to western sound (Ho et al., 2019). Moreover, Ho et al., (2019) reported the occurrence of submarine groundwater discharge (SGD) as another possible freshwater input to the WMS area. Additionally, freshwater from outflows of the Pearl River and the diverted Mississippi River water, during flood

situations, through the Bonnet Carre Spillway via Lake Pontchartrain brings in freshwater and a high concentration of nutrients that sometimes proves detrimental to the oysters.

3.2.1.2 Anthropogenic point sources

The two coastal counties named Hancock and Harrison, and its residential areas are effectively contributing to anthropogenic pollutants to the study area. Additionally, the study area is influenced by sewer outfall from the Hancock County located west of BSL and the effluents from the DuPont DeLisle titanium dioxide plant located north of BSL. This plant has an effluent pipe which releases waste directly into BSL (EPA 2010b). Further, in the eastern side of the BSL, the Industrial Park located in Harrison County in Pass Christian is another vital point source where many companies discharge effluents to the creaks and bayous adjacent to the Bay.

3.2.2 Sample collection

A total of 45 samples were collected during March, May, June, and July 2018 (Fig. 3.1, Table 3.1). Only surface samples were collected during March, while May, June, and July and sampling included surface, middle, and bottom water samples. Surface samples were collected by using a sampling stick from a non-agitated water surface while the bottom and middle layer samples were collected using a Niskin Bottle. Water samples were collected using acid-washed 500 ml polyethylene bottles and stored in cooler filled with ice and transported to the laboratory within 2-4h of collection. *In-situ* physicochemical parameters including temperature, salinity, and DO profiles were measured using a Hanna multiparameter probe (HI9828, Hanna Instruments, RI). For dissolved inorganic carbon (DIC), pH, total alkalinity (*TAlk*), and salinity measurements, water samples were collected from the surface, middle, and bottom waters during May, June and July, and only surface samples were collected during the March field campaingn. Samples were

collected using a Niskin water sampler , with water samples transferred directly into glass bottles via silicon tubing (Dickson et al., 2007), and 25µl of $HgCl_2$ was added immediately after collection in acid-washed glass bottles. Samples were stored in cooler with ice and sent to the Center of Applied Coastal Research, University of Delaware, USA.

Table 3.1 Summary of field trips, water sample, and *in situ* data collection.

Sampling Trips	Date	Number of Samples
1	6-8 March 2018	9
2	7-12 May 2018	19
3	18-20 June 2018	9
4	16-20 July 2018	6

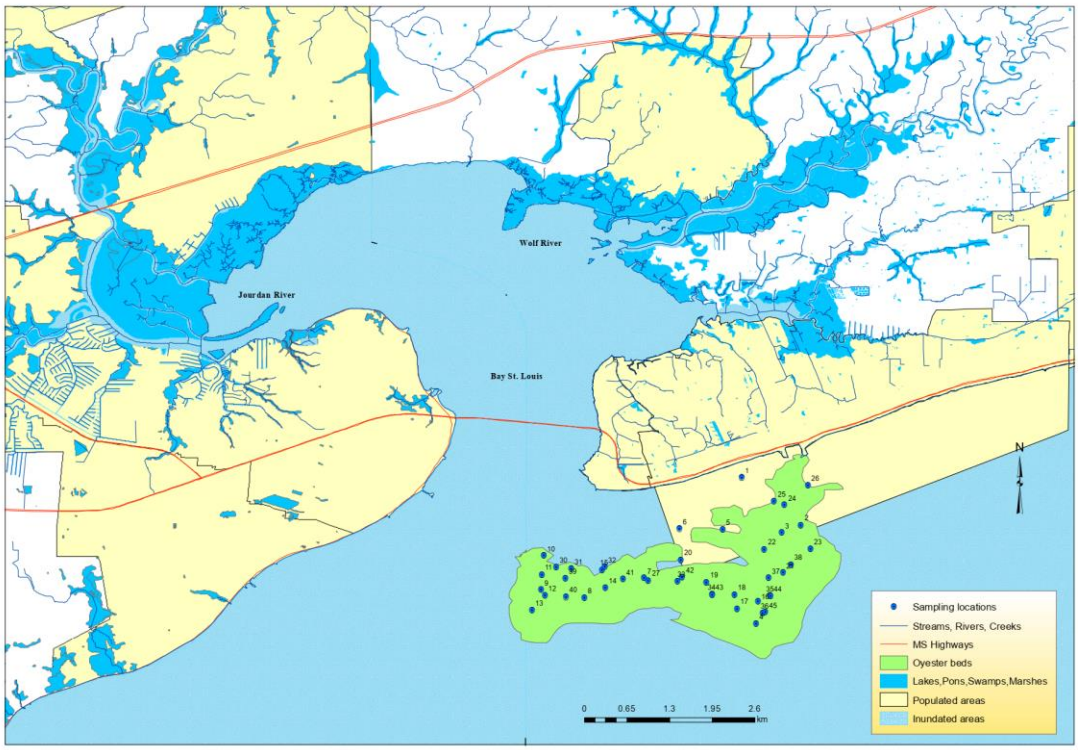

Figure 3.1 Map of the study area.

3.2.3 Analytical methods

3.2.3.1 Nutrients and cations

For nutrient analysis, aliquots of water samples were filtered using 47 mm diameter (Nucleopore, 0.7 µm) filters. The filtrate was stored in 20ml HDPE bottles in -80 °C for DOC, TDN, PO_4^{3-}, NO_3^-, NO_2^-, and NH_4^+ analyses. DOC and TDN concentrations were measured using a Shimadzu TOC-TNM1 total organic carbon-total nitrogen analyzer equipped with an ASI-V auto ampler as described by Shang et al. (2018) at University of Alabama and the anions were analyzed using a continuous flow auto-analyzer (Skalar Analytical Inc., Buford, GA) at Dauphin Island Sea Lab.

3.2.3.2 Spectral absorption coefficients of CDOM

The collected water samples were filtered using 0.2 µm Nucleopore membrane filters under low vacuum. Filtered samples were stored at 4 ^{o}C in acid cleaned, pre-combusted amber colored glass bottles for laboratory analysis. Sample analysis was carried out by following the analytical procedures mentioned by Singh et al., (2017). For absorbance measurements ($a_{CDOM}(\lambda)$), first samples were kept in room temperature to reach ambient temperature. Then absorbance between 400 nm to 750 nm was measured with 2 nm intervals and absorbance values were corrected by using the absorbance of freshly collected nano-pure Milli-Q water (Goncalves et al., 2018). Absorption coefficient of CDOM were calculated by following the methods explained by Matsuoka et al., (2012) and Matsuoka et al., (2015).

3.2.3.3 Dissolved trace metals, DIC, and *TAlk*

Analysis of trace metals including, arsenic (As), manganese (Mn), zinc (Zn), copper (Cu), mercury (Hg) uranium (U) and iron (Fe) were performed using inductively coupled plasma mass spectrometry (ICP-MS). DIC and *TAlk* were analyzed in the Center of Applied Coastal Research, University of Delaware, USA in Dr. Cai's laboaratory according to Dickson et al. (2007) and Riebesell et al. (2010).

3.3 Results and discussion

3.3.1 Variations of hydrographic parameters

River gauge heights of WR and JR were obtained from the USGS gauge stations on the WR (USGS 02481510) and JR (USGS 02481660) during the sampling period (Fig.3.2; Table 3.2). The highest gauge height of WR reported during March trip (206.6 ± 3.7 cm) while the lowest gauge height reported during the June trip (172.9 ± 1.9 cm). Gauge heights form JR showed the

highest precipitation in March field trip (29.6 ± 0.5 cm) and lowest in May (21.7 ± 3.8 cm). These discharge patterns suggest the influence of seasonal induced local precipitation patterns in the study region similar to that reported by Ho et al. (2019).

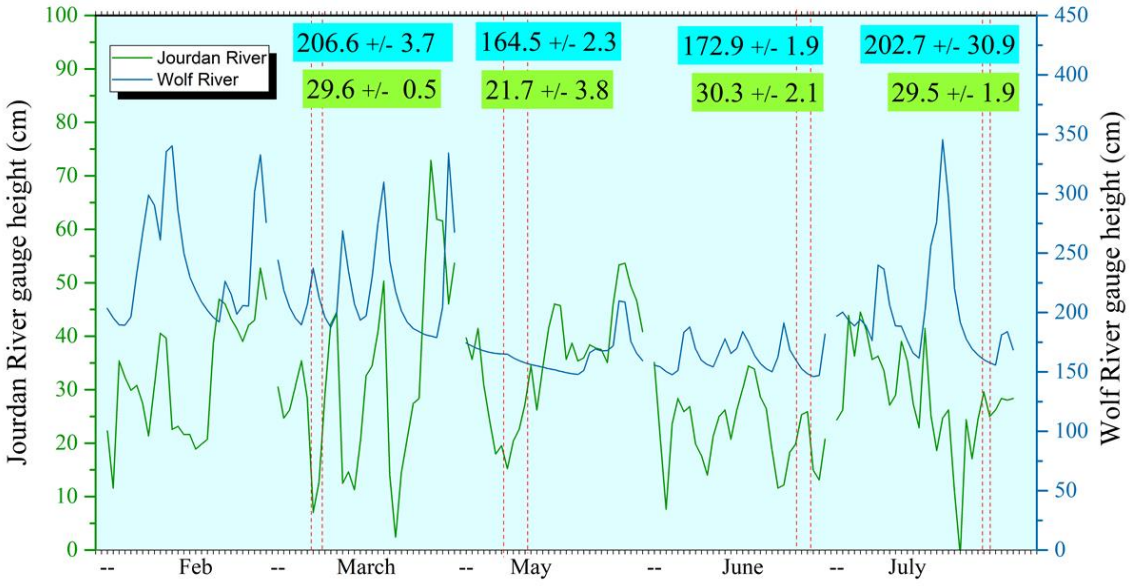

Figure 3.2 Time series of Jourdan River (green) and Wolf River (blue) gauge heights recorded at gauge stations USGS 02481660 on the Jourdan River near Bay St Louis and USGS 02481510 on the Wolf River near Landon, MS.

Observed average gauge heights of JR shows a significant correlation with observed average salinity through March to July (Table 3.2). Specifically, considerable salinity variations appear because of the mixing of saline coastal waters with fresh water discharge from rivers (Keith et al., 2015). Variation in salinity can influence conservative mixing of the biological and chemical substances vertically as well as horizontally across shelf areas (Miller et al. 1998). Moreover,

salinity is responsible for biogeochemical processes as well as creating biological and chemical gradients both horizontally and vertically within the water column (Keith et al., 2015).

Table 3.2 Monthly mean water level from the USGS gauges for the Wolf River and Jourdan River, Mississippi.

Dates	Gauge Height (average) (cm)		Discharge (average)(m3/s)	
	Wolf River	Jourdan River	Wolf River	Jourdan River
6-8, March 2018	206.6	29.6	19.97	n/a
7-12, May 2018	164.5	21.7	3.76	n/a
18-20,June 2018	172.9	39.3	4.60	n/a
16-20,July 2018	202.7	29.5	13.81	n/a

*Average gauge heights were calculated by considering the residential time of BSL (Sawant, (2009))
n/a refers to data not available
Source: https://waterdata.usgs.gov/nwis

The measured surface water temperature (SWT) varied from 25.66 to 31.72°C through the study period (Fig. 3.3; Table 3.3). The highest average SWT observed during the summer period (28.02 ± 1.52 °C), and the lowest SWT reported during spring as 16.09 ± 0.37 °C. Measured averaged mid-depth, and bottom water temperatures were 27.54 ± 1.75 °C and 27.29 ± 1.70 °C respectively, during the summer period. Measured average temperature values showed a decreasing trend from surface to bottom waters (Table 3.3). Generally, this type of vertical temperature distribution can occur due to energy transferring processes (e.g., solar radiation) and advective transfer processes of tides and currents in the water column (LaFond, 1954).

In this study, measured surface salinity varied from 3.90 psu to 20.10 psu from spring to summer. Averaged surface salinity showed an increasing trend with temporal variation from spring (4.76 ± 1.10 psu) to summer (13.00 ± 3.55 psu) (Table 3.3, Fig. 3.3).

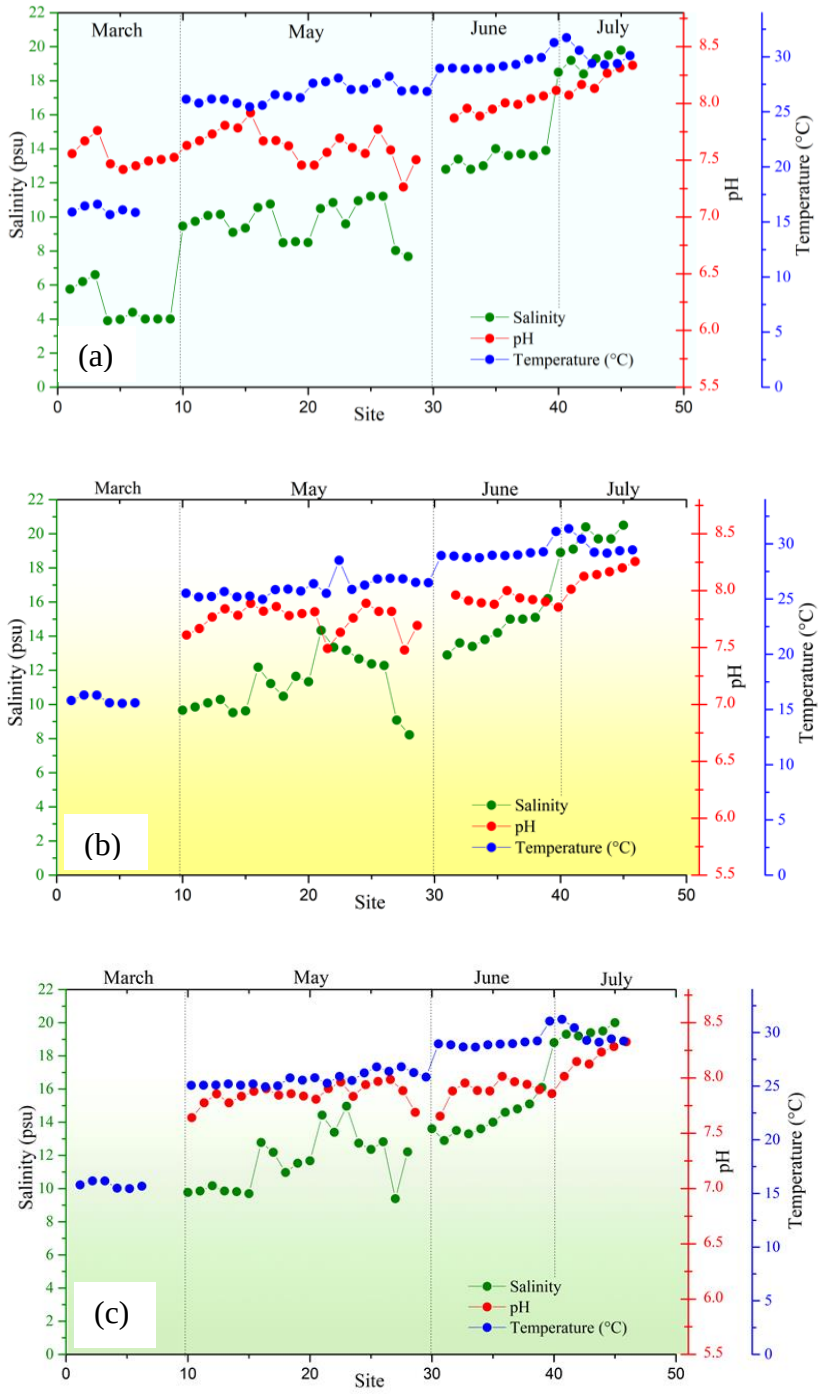

Figure 3.3 Variation of (a) surface, (b) Mid-depth, and (c) bottom layer salinity, temperature, and pH during March, May, June, and July 2018.

.

During summer, the highest average salinity observed in bottom waters (14.40 ± 6.85 psu) while lowest observed in surface waters (13.00 ± 7.50 psu). (Table 3.3, Fig 3.3 (a) and (b)). Table 3.3, Fig 3.3 (a) and (b)). In addition, surface salinity and temperature showed a strong positive correlation $R^2 = 0.6348$ and $R^2 = 0.6859$ during spring and summer season, respectively (Fig. 3.4). The observed positive correlation between surface salinity and temperature suggests the influence of fresh/cooler water in the spring as a result of higher discharge and saline/warmer water during summer. This type of behavior could be occurred due to high local precipitation during March while high evaporation condition during May, June, and July. Further, temperature and salinity can significantly regulate the ocean water density and consequently affect most of the biogeochemical processes in the water column.

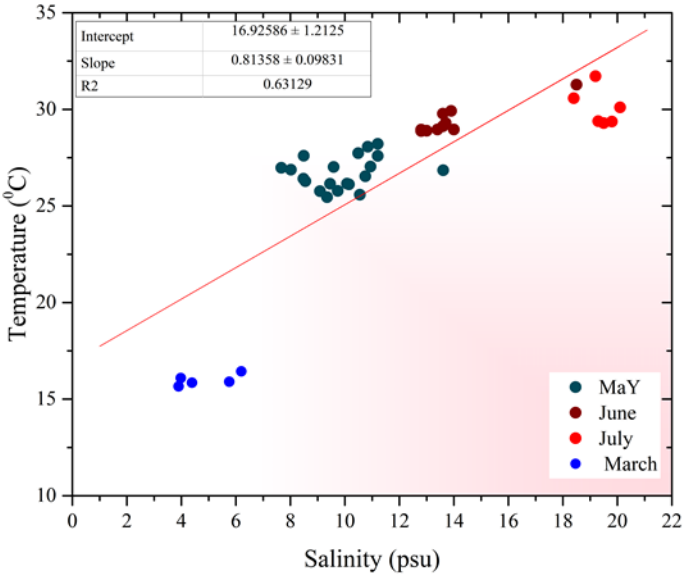

Figure 3.4 Variation of surface temperature and salinity during (a) May, June, and July (b) March.

Measured surface pH values indicated a general increasing trend during spring to summer, 7.54 ± 0.11, and 7.85 ± 0.23, respectively (Table 3.3, Fig. 3.3). Similarly, both middle and bottom water pH values showed an increase in pH values with depth, as shown in figure 3.3 (b) and (c), respectively. This type of specific behavior could be appeared due to ocean circulation and microbial activities, which controls the pH levels in the oceanic water column. In coastal waters the magnitude of pH may depend on various factors such as alkalinity, dissolved carbon dioxide concentrations and H^+ ion concentrations. Generally, pH increases until saturation of $CaCO_3$ happen while pH values decrease due to the mixing of fresh water (pH 7.0-7.5) with saltwater (pH 8.2 coastal water), especially in coastal waters (Radke, 2002). Further, during organic matter decomposition processes, a substantial amount of water DO will consume and as result of that CO_2 will be produce. This process considered a natural event that can reduce the water pH in coastal waters.

Table 3.3 Physicochemical parameters of coastal water and measured absorption coefficients and spectral slopes of CDOM. Parameters showed with respect to seasons and depths of this study.

	surface				Middle				Bottom			
Season	**Min.**	**Max.**	**Mean**	**S.D**	**Min.**	**Max.**	**Mean**	**S.D**	**Min.**	**Max.**	**Mean**	**S.D**
Spring												
Temperature (°C)	15.66	16.61	16.09	0.37								
Salinity (psu)	3.9	6.61	4.76	1.1								
pH	7.42	7.76	7.54	0.11								
DO (ppm)	n/a	n/a	n/a	n/a								
DOC (mg/L)	4.93	5.06	4.93	0.16								
DIC (µM/kg)	571	767	641	71								
a_{CDOM} **(440)**	0.008	0.014	0.010	0.002								
a_{CDOM} **(412)**	0.013	0.032	0.014	0.006								
S_{CDOM}	0.006	0.017	0.013	0.004								
Summer												
Temperature (°C)	25.46	31.72	28.02	1.7	24.98	31.37	27.54	1.895	24.94	31.22	27.29	1.7
Salinity (psu)	7.67	20.10	13.00	3.75	8.22	21.2	14.3	3.82	9.39	21.3	14.4	3.425
pH	7.26	8.34	7.85	0.23	7.48	8.26	7.89	1.26	7.64	8.33	7.94	0.15
DO (ppm)	5.54	7.8	6.63	0.65	3.17	6.71	5.13	1.01	1.23	6.39	4.48	1.455
DOC (mg/L)	3.73	4.38	4.04	0.20	n/a	n/a	n/a	n/a	n/a	n/a	n/a	n/a
DIC (µM/kg)	858	1620	1220	196	920	1660	1320	231.5	948	1660	1340	197.5
a_{CDOM} **(440)**	0.004	0.013	0.007	0.003	n/a	n/a	n/a	n/a	n/a	n/a	n/a	n/a
a_{CDOM} **(412)**	0.007	0.029	0.010	0.006	n/a	n/a	n/a	n/a	n/a	n/a	n/a	n/a
S_{CDOM}	0.008	0.019	0.014	0.004	n/a	n/a	n/a	n/a	n/a	n/a	n/a	n/a

*n/a = data not available

3.3.2 Variation of DOC and absorption coefficient of CDOM

Measured surface DOC concentrations ranged from 3.73 mg/L to 5.06 mg/L during May and March field trips. Highest average DOC concentration was reported during March trip (4.93 ± 0.16 mg/L) while the lowest reported during May (4.04 ± 0.20 mg/L). Further, DOC showed a strong negative correlation (R^2 = 0.851) with salinity indicating the conservative mixing nature of DOC in the study area (Fig. 3.5 (a)). Especially marine DOC considers as the primary intermediate in carbon transfers in oceanic food webs (Doval and Hansell, 2000) and DOC use as a fundamental

element of ocean carbon models (Thingstad and Rassoulzadegan, 1999). Generally, DOC and salinity relationship appears to be more complex and can strongly affect the occurrence of various DOC concentrations in the different water masses (Seritti et al., 2003). Figure 3.5(b) shows a strong positive correlation ($R^2 = 0.881$) between salinity and measured DIC in this study. In aquatic systems, DIC represents the total concentration of all dissolved inorganic carbon compounds, including CO_2 (aq), CO_3^{2-} and HCO_3^-. This unique nature could potentially due increasing of dissolved CO_2 as a result of photosynthesis processes observed in the surface water column.

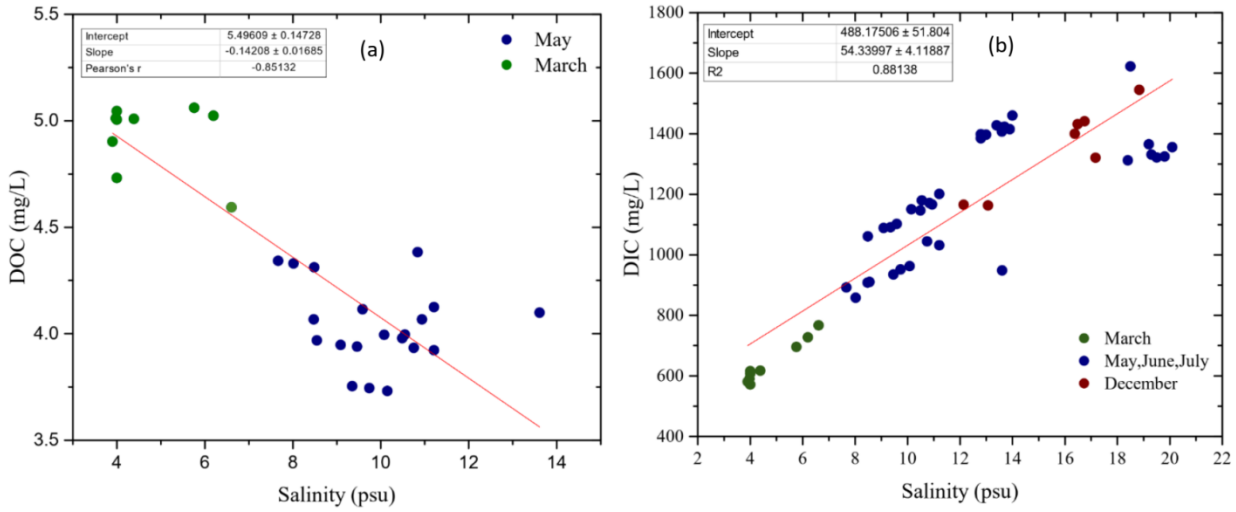

Figure 3.5 Variation of (a) Surface salinity and DOC during March and May (b) surface salinity and DIC during March, May, June, and July.

3.3.3 CDOM spectral measurements

The measured a_{CDOM} (440) varies from 0.0040 m^{-1} to 0.0140 $m^{-1,}$ with an average value of 0.0095 ± 0.0075 m^{-1} throughout the study (March- July). However, samples collected from summer season showed an average of 0.0070 ± 0.0030 m^{-1} while comparably a higher average value (0.0100± 0.0020 m^{-1}) observed from samples collected during the spring period. The observed

variation of a_{CDOM} with salinity can use as another proxy is to determine the temporal variation of CDOM in coastal waters (Macdonald et al., 1989; Matsuoka et al., 2012). However, a positive correlation (R^2 = 0.3244) observed for samples collected during summer and samples collected during the spring period showed a weak negative relationship (R^2 = 0.2533) (Fig.2.8).

A similar negative relationship of a_{CDOM} and salinity observed by Fichot et al. (2016) in the NGoM region and this types of characteristics nature exist due to the nature of physical mixing of freshwater and oceanic end-members and regulation of DOM concentrations in coastal waters (Fichot et al., 2016). Additionally, this type of variance can occur possibility due to a relatively unaltered terrigenous CDOM end-member from rivers, and a photochemically altered terrigenous CDOM end-member from coastal regions (Benner and Opsahl, 2001; Hernes and Benner, 2003; Fichot and Benner, 2012).

The spectral slope of CDOM (S_{CDOM}) calculated by fitting a non-linear regression to the absorbance data from 350 to 500 nm, followed by Babin et al., (2003). The calculated spectral slope of CDOM absorption range from 0.0060 nm^{-1} to 0.0190 nm^{-1} where lowest and highest values were reported spring (WMS-6) and summer (WMS-34) respectively. The calculated S_{CDOM} for the spring season was lower (0.0130 ± 0.0040 nm^{-1}) compared to S_{CDOM} observed (0.0140 ± 0.0040 nm^{-1}) during the summer season. Samples collected during spring season showed a lowest salinity (4.76 ± 1.10 psu), highest a_{CDOM} (412) (0.014 ± 0.006 m^{-1}), and lowest mean spectral slope (0.0013 ± 0.0040 nm^{-1}) values. By contrast, highest salinity (13.00 ± 3.75 psu), lowest a_{CDOM} (412) (0.0010 ± 0.0060 m^{-1}), and highest CDOM spectral slope (0.014 ± 0.004 nm^{-1}) observed samples collected May, June and July trips. The measured spectral slopes of CDOM can use as a proxy for estimating the average molecular sizes of DOM, where higher the spectral slope indicates the

existence of low molecular weight DOM and vice versa (Helms et al., 2008). Moreover, the molecular size, in turn, has been linked to the bioavailability and reactivity of DOM (Tranvik,1990; Amon and Benner, 1996). Further magnitude of the S_{CDOM} can vary due to bulk sources or local processes of DOM (Carder et al., 1989; Blough and Del Vecchio.2002).

The observed bio-optical properties indicate increasing of photo-bio degradation of DOM from spring to summer season (Johi and Eurico, 2015). Especially, high levels of both a_{CDOM} and DOC in spring suggest the influence of OM rich water sources (Matsoka et al., 2012) while low levels of a_{CDOM} and DOC indicates the microbial and photodegradation of OM in coastal waters (Moran et al., 2000; Helms et al., 2008; Christoper et al., 2009). Especially photobleaching due to the effect of sunlight is considered as an important mechanism that can remove DOM from surface coastal waters (Miller and Zepp 1995; Vodacek et al. 1997). Additionally, increased solar insolation and reduced periods of strong winds in the summer periods provide favorable conditions for photochemical reactions (Blough, 2002, Vodacek et al., 1997). The analyzed a_{CDOM} showed a spatial and seasonal variation influenced by various factors as described by previous studies (Joshi and Eurico, 2015) such as seasons, river discharge (CDOM rich freshwater) precipitation/run-off and strong winds.

Christoper et al., (2009) demonstrated that increasing salinity does not affect photobleaching of river and estuarine a_{CDOM} at short wavelengths (e.g., 280 nm) but photobleaching of a_{CDOM} at longer wavelength enhanced with salinity. Thus, sunlight photobleaching is being considered as an essential DOM removal mechanism of the coastal waters (Vodacek et al. 1997). Consequently, photochemical processes control the constituents of carbon cycling in marine environments where sunlight influenced converted DOM brings inorganic forms

of carbon constituents to the water column (Moran et al., 2000). For example, DIC, carbon monoxide (CO) and bacterial substrates (low-molecular-weight carbonyl compounds and others) increase turnover rates of DOM in surface waters as a result of photochemical reactions (Bushaw et al. 1996; Miller and Moran 1997; Moran and Zepp 1997).

3.3.4 Trace metal distribution

Majority of trace metals showed a strong positive correlation with salinity where higher trace metal concentrations were observed in summer season (Co, Ni, Zn, As, Sb, Se, and U) (Table 3.4). However, Pb and As concentrations were higher in the spring season and reduced during summer period resulting in a strong negative correlation possibly due to inputs from industrial influences around BSL area (Fig. A.1). Incidentally, some trace metals such as Hg, Cr, Mn, and Cu do not show any specific relationship along with seasonal changes and a similar result reported by Joung and Shiller, (2016).

Measured Co concertation range from 0.47 – 2.81 ppb with an average value of 1.62 ± 1.44 ppb from March to July. The observed Co distribution in surface water appears to be a conservative mixing behavior where dissolved Co and salinity showed a robust positive correlation ($R^2 = 0.885$), and this could be possibly due to upward mixing nature of Co enriched bottom waters during vertical mixing process (Fig.3.6).

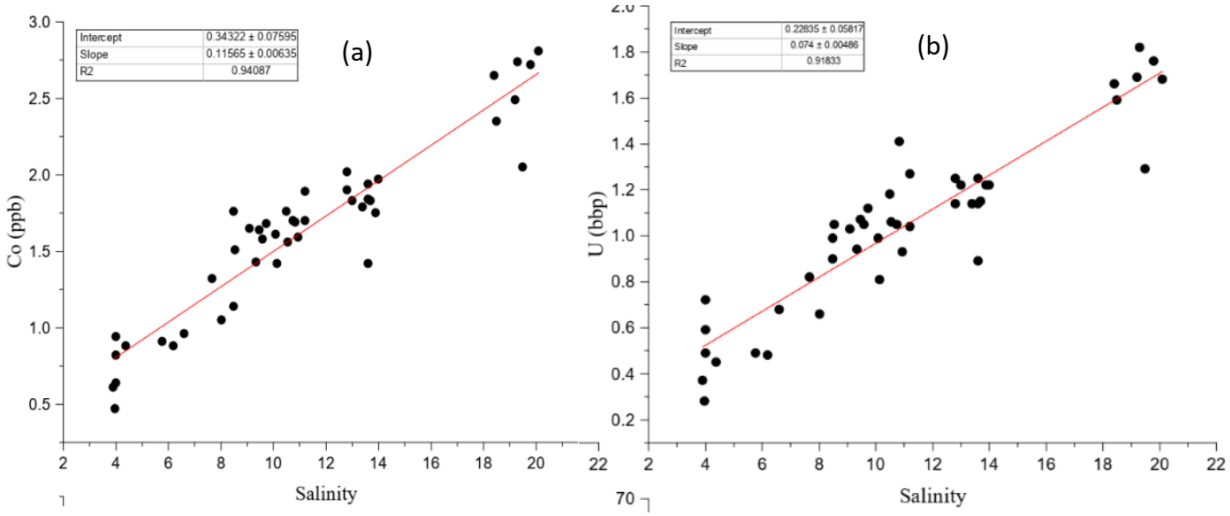

Figure 3.6 Variation of measured (a) Co and (b) U concentrations with respect to salinity for the study area samples were collected during March, May, June, and July 2018.

A similar observation was reported by Joung and Shiller (2016), where higher Co concentration was observed with higher salinity stations, especially during the summer season. Previous studies had reported the conservative mixing nature of U in Mississippi Sound (Joung and Shiller, 2016; Ho et al., 2019). During this study U concentrations showed an increasing trend from March (0.48 ± 0.26 ppb) (spring) to July (1.18 ± 0.56 ppb) (summer) showing a conservative mixing with surface salinity (R^2 = 0.843) (Fig.3.6). Observed Co concentration showed a similar trend as U on surface waters. This behavior could be most likely due to episodic vertical mixing, and a similar observation was observed in Louisiana Self waters by Joung and Shiller, (2016).

Naturally, in aquatic systems, toxic metals are transported either in dissolved or particulate form, where sediment and suspended particles play essential roles in metal adsorption, desorption, and dissolution, and sedimentation processes (Boyle et al., 1974, Gonzalez et al., 2007). However, these processes being regulated by natural phenomena's such as estuarine circulation, river and groundwater discharge, tidal flooding, sediment input, and re-suspension, exchange with

neighboring environments, water properties (e.g. salinity, redox and pH) and the presence of organisms jointly determine the mobility of metals (Machado et al., 2016). Notably, rivers considered as the primary sources of transportation of terrestrial-derived trace metals to the coastal environments (Pan and Wang, 2012).

Table 3.4 Concentrations of microelements and heavy metal contents of samples collected during spring and summer.

	Cr52	Mn55	Co59	Ni60	Cu65	Zn66	As75	Se78	Sb123	Pb208	U238
Spring											
Min.	2.85	5.53	0.47	7.54	3.06	2.21	27.95	0.98	0.00	0.00	0.28
Max.	5.35	33.58	0.96	12.71	12.79	20.16	48.51	6.41	0.00	1.10	0.68
Mean	3.62	14.58	0.76	10.94	7.63	6.61	36.19	3.20	0.00	0.62	0.48
S.D.	1.71	20.19	0.38	3.45	8.09	12.40	18.07	4.08	0.00	0.92	0.26
Summer											
Min.	2.99	0.00	1.05	12.55	4.69	4.41	54.81	0.00	0.00	0.00	0.66
Max.	6.77	63.80	2.81	24.93	12.97	20.18	154.26	13.79	0.47	0.84	1.82
Mean	4.17	17.50	1.83	18.75	8.92	11.30	92.49	5.40	0.19	0.40	1.18
S.D.	1.69	34.24	0.86	5.66	3.89	7.77	54.73	7.48	0.24	0.55	0.56

All the concentrations were measured in ppb level.

3.3.5 Distribution of DO and biogeochemical processes

During this study, DO concentrations available only for the May sampling trip. However, in May sampling, lowest and highest DO measurements were reported in the bottom and surface water samples as 1.23 ppm and 7.80 ppm, respectively (Table 3.3). By considering the observed DO values, it can interpret that bottom DO concentrations were close to the hypoxic conditions which observed at WMS 29 (DO = 1.23 ppm) during the May sampling trip. The tendency for stratification, the rate of flushing, and the extent of organic loading effectively control the potential occurrences of hypoxia coastal environments (Engle et al., 1999). More importantly, stratification is related to water depth, freshwater inflow, and tidal energy (Nelson et al., 1994). Mortality of organisms and decreasing of habitat carrying capacity control the presence of hypoxic conditions

(Diaz and Solow, 1999). Additionally, the presence of hypoxic and anoxic conditions reduce demersal fish stocks (Breitburg, 1990) and mortality of aquatic organisms such as oysters (Lenihan and Peterson, 1995). Prolonged depletion of DO concentration and areal expansion of bottom water hypoxia observed in the NGoM (Rabalais et al., 2002) and continuation of this processes can disrupt benthic communities (Flemer et al., 1999).

3.3.6 Biogeochemical influences

The concept of alkalinity normalization is widely utilized for correct *TAlk*, and salinity changes caused due to precipitation and evaporation in ocean water studies (Friis et al., 2003; Robbins et al., 2001). The normalized total alkalinity (n*TAlk*) can be obtained as *TAlk*/Salinity multiplied by a reference salinity of 35 psu or an average salinity value (Challener et al., 2016). In this study, average salinity values of 12.60 psu, 13.90 psu, 13.70 psu used as the reference for calculating surface, mid-depth, and bottom n*TAlk*, respectively. All the average salinity values were calculated by considering the summer samples where precipitation appears to be minimal compared to spring.

The calculated surface n*TAlk* ranged from 1050 µM/kg to 1990 µM/kg from summer to spring period. Similarly, the lowest nDIC (858 µM/kg) was observed during summer and highest (1940 µM/kg) observed in the spring sampling period (Table 3.5). The calculated mid-depth nDIC and n*TAlk* ranged from 920 µM/kg to 1660 µM/kg and 1090 µM/kg to 1940 µM/kg respectively. Furthermore, normalized bottom nDIC and n*TAlk* ranged from 948 µM/kg to 1660 µM/kg and 1130 µM/kg to 1940 µM/kg respectively. However, in summer, both average nDIC (1300 ± 193 µM/kg) and n*TAlk* (1460 ± 231 µM/kg) slightly higher in bottom waters compared to surface water nDIC and n*TAlk*, 1280 ± 266 µM/kg and 1440 ± 273 µM/kg.

Table 3.5 Concentration of DIC and *TAlk* after normalizing based on the average salinity of each season.

	Surface		Middle		Bottom	
	nDIC	**n*TAlk***	**nDIC**	**n*TAlk***	**nDIC**	**n*TAlk***
Spring						
Min.	1460	1520				
Max.	1940	1990				
Mean	1730	1780				
S.D.	195	194				
Summer						
Min.	858	1050	920	1090	948	1130
Max.	1620	1840	1660	1940	1660	1940
Mean	1200	1380	1280	1440	1300	1460
S.D.	202	262	226	273	193	232

All the measured values are in µM/kg

A graphical representation of nDIC and n*TAlk* introduced by Deffeyes (1965) can explain the important biological processes such as processes, including photosynthesis, respiration, carbonate precipitation and dissolution, and gas exchange (Suzuki and Kawahata, 2003). Seasonally normalized DIC and *TAlk* values for surface samples of WMS region reflect the possible metabolic process including net calcification and dissolution, photosynthesis and respiration.

Figure 3.7 shows that photosynthesis and calcification processes are prominent during summer while calcification and respiration process prominent in spring. This type of behavior possibly occurred due to the removal of CO_2 from the surface water column as a result of photosynthesis and $CaCO_3$ formation (Gattuso et al., 1999) (E.q 3.1 and 3.3). Furthermore calcification can reduce DIC concentration by consuming CO_3^{2-} and HCO_3^- ions to form $CaCO_3$ as explained by WolfGladrow et al. (2007) (Eq.3.7). Primarily, more elevated CO_2 levels also can attribute to the calcification process (Kawahata et al., 1997; Suzuki and Kawahata, 2003). According to the Eq.3.2, photosynthetic process can increase the OH^- ion capacity in the water

column and resulting in favorable condition for calcification Eq.3.3. These two processes can act as a linked loop where consumption of CO_2 and releasing of CO_2 will behave together.

Organic carbon metabolism;

Photosynthesis (CO_2 invasion):

$$HCO_3^- + H_2O \rightarrow CO_2 + OH^- + H_2O \rightarrow CH_2O + OH^- + O_2 \quad (3.1)$$

Respiration/degradation (CO_2 evasion):

$$CH_2O + O_2 \rightarrow CO_2 + H_2O \quad (3.2)$$

Inorganic carbon metabolism;

Calcification (CO_2 evasion):

$$Ca^{2+} + 2HCO_3^- + OH^- \rightarrow Ca^{2+} + CO_3^{2-} + H^+ + OH^- \rightarrow CaCO_3 + H_2O + CO_2 \quad (3.3)$$

Dissolution of carbonate (CO2 invasion):

$$CaCO_3 + H_2O + CO_2 \rightarrow Ca^{2+} + 2HCO_3^- \quad (3.4)$$

During the summer period, consumption of CO_2 (with H_20) increases due to photosynthesis with increased temperature in the thermocline region (Eq. 3.1). As a result of photosynthesis, the formation of glucose and O_2 occur. Glucose used as the energy source for the metabolism of the plankton cell. Furthe, due to metabolism, planktons can generate other organic compounds (Eq. 3.1). With produced nutrients, phytoplankton community can grow and multiply. Eventually, the plankton and the animals that feed on them die and sink into deeper water, where they decompose through microbial degradation. Microbial degradation of OM requires DO, especially in bottom waters (E.q. 3.2). Apart from in situ produced OM, terrestrial inputs also bring a significant amount of nutrients to the system. Hence, microbial activities are prominent in water column, especially

in the spring season. As a result of excessive microbial respiration, elevated levels of CO_2 can observe, which potentially causes reduced pH levels (E.q 3.2). Dissolution of CaCO3 prominent with low pH waters, which observed during the spring season. The observed n*TAlk* and nDIC values of the study area reflect that both calcification and photosynthesis may occur in summer while spring data indicate that respiration and dissolution (Cyronak et al., 2018)

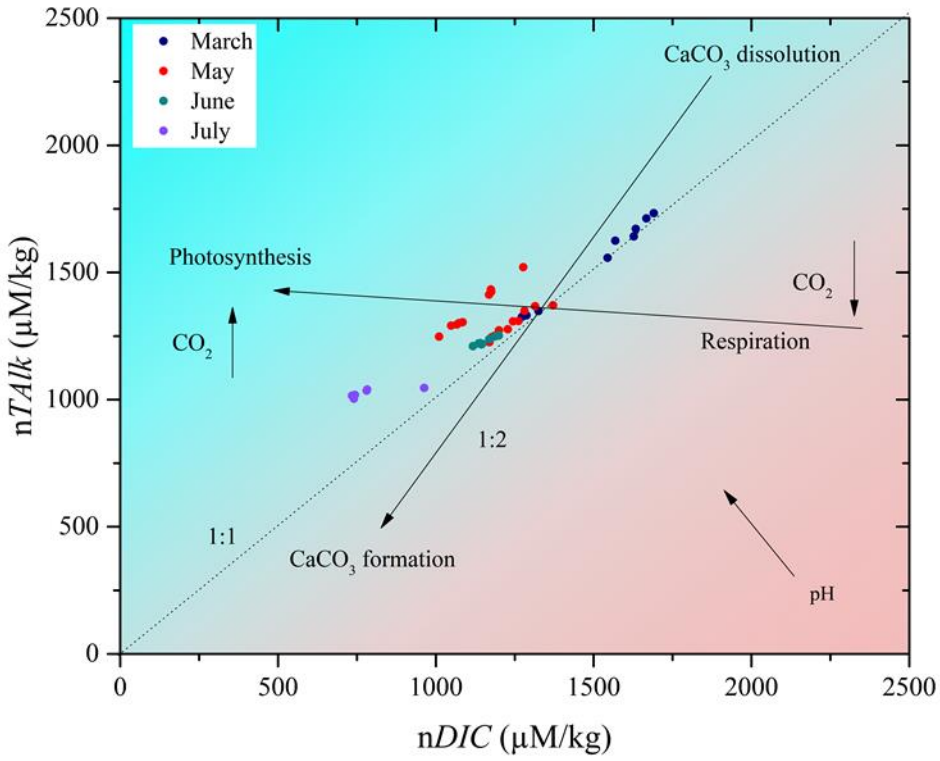

Figure 3.7 Normalized dissolved inorganic carbon concentrations (nDIC) versus the normalized total alkalinity (n*TAlk*) measured during the study. The arrows show the impacts of the mentioned processes on the nDIC concentration and the n*TAlk*.

3.4 Conclusions

The observed results in this study indicate that seasonal processes influence the DOM distributions in the WMS region potentially due to riverine inputs during the spring season. Increased DOC and a_{CDOM} levels together with low DIC suggest the inputs of organic matter while lower S_{CDOM} suggests the presence of larger organic molecules during higher discharges in the spring season. However, during summer, reduced DOC and a_{CDOM} levels were observed together with high DIC concentrations. Similarly, high S_{CDOM} suggest the presence of small organic molecules. This type of behavior could be observed due to increased bio-photodegrading activities during the summer period. Higher concentrations of toxic metals together with higher DOM, indicates incorporation of trace metals in DOM, which increases the chance for toxic metals to be bioaccumulated in benthic organisms, especially in filter feeders. Observed results indicate that respiration and dissolution of $CaCO_3$ were prominent in the spring season with lower pH levels while photosynthesis and formation of $CaCO_3$ prominent during summer periods. Reduced levels of DO observed during summer season compared to spring periods. Potential hypoxic conditions could occur with the favorable conditions explained. Since DOM is associated with most of the biogeochemical processes in coastal waters, DOM can utilize as a proxy to understand the behavior of the environmental factors affecting oyster health. Hence, estimation of DOM over will provide a better understanding for protecting the Henderson Point and Pass Christian Oyster reefs.

3.5 REFERENCES

Amon, R.M. and Benner, R., 1996. Bacterial utilization of different size classes of dissolved organic matter. Limnology and Oceanography, 41(1), pp.41-51.

Babin, M., Stramski, D., Ferrari, G.M., Claustre, H., Bricaud, A., Obolensky, G. and Hoepffner, N., 2003. Variations in the light absorption coefficients of phytoplankton, nonalgal particles, and dissolved organic matter in coastal waters around Europe. Journal of Geophysical Research: Oceans, 108(C7).

Benner, R., Pakulski, J.D., McCarthy, M., Hedges, J.I. and Hatcher, P.G., 1992. Bulk chemical characteristics of dissolved organic matter in the ocean. Science, 255(5051), pp.1561-1564.

Benner, R. and Opsahl, S., 2001. Molecular indicators of the sources and transformations of dissolved organic matter in the Mississippi River plume. Organic Geochemistry, 32(4), pp.597-611.

Benner, R., 2002. Chemical composition and reactivity. Biogeochemistry of marine dissolved organic matter, 3, pp.56-90.

Bilby, R.E. and Likens, G.E., 1979. Effect of hydrologic fluctuations on the transport of fine particulate organic carbon in a small stream1. Limnology and Oceanography, 24(1), pp.69-75.

Blough, N.V. and Del Vecchio, R., 2002. Biogeochemistry of marine dissolved organic matter. Chromophoric DOM in the coastal environment in, pp.509-546.

Breitburg, D.L., 1990. Near-shore hypoxia in the Chesapeake Bay: patterns and relationships among physical factors. Estuarine, Coastal and Shelf Science, 30(6), pp.593-609.

Bolan, N.S., Adriano, D.C., Kunhikrishnan, A., James, T., McDowell, R. and Senesi, N., 2011. Dissolved organic matter: biogeochemistry, dynamics, and environmental significance in soils. In Advances in agronomy (Vol. 110, pp. 1-75). Academic Press.

Boyle, E., Collier, R., Dengler, A.T., Edmond, J.M., Ng, A.C. and Stallard, R.F., 1974. On the chemical mass-balance in estuaries. Geochimica et Cosmochimica Acta, 38(11), pp.1719-1728.

Brunner, C.A., Beall, J.M., Bentley, S.J. and Furukawa, Y., 2006. Hypoxia hotspots in the Mississippi Bight. The Journal of Foraminiferal Research, 36(2), pp.95-107.

Bushaw, K.L., Zepp, R.G., Tarr, M.A., Schulz-Jander, D., Bourbonniere, R.A., Hodson, R.E., Miller, W.L., Bronk, D.A. and Moran, M.A., 1996. Photochemical release of biologically available nitrogen from aquatic dissolved organic matter. Nature, 381(6581), pp.404-407.

Carder, K.L., Steward, R.G., Harvey, G.R. and Ortner, P.B., 1989. Marine humic and fulvic acids: Their effects on remote sensing of ocean chlorophyll. Limnology and oceanography, 34(1), pp.68-81.

Cai, Y., Guo, L., Wang, X., Mojzis, A.K. and Redalje, D.G., 2012. The source and distribution of dissolved and particulate organic matter in the Bay of St. Louis, northern Gulf of Mexico. Estuarine, Coastal and Shelf Science, 96, pp.96-104.

GULF COAST RESEARCH LABORATORY (GCRL). 1978. Environmental baseline survey, St. Louis Bay. Gulf Coast Research Laboratory, Ocean Springs,Mississippi.

Challenger, R.C., Robbins, L.L. and McClintock, J.B., 2016. Variability of the carbonate chemistry in a shallow, seagrass-dominated ecosystem: implications for ocean acidification experiments. Marine and Freshwater Research, 67(2), pp.163-172.

Chen, R.F. and Gardner, G.B., 2004. High-resolution measurements of chromophoric dissolved organic matter in the Mississippi and Atchafalaya River plume regions. Marine Chemistry, 89(1-4), pp.103-125.

Christopher, L., O'Sullivan, D.W. and Boyd, T.J., 2009. Increases in the longwave photobleaching of chromophoric dissolved organic matter in coastal waters. Limnology and Oceanography, 54(1), pp.145-159.

Cyronak, T., Andersson, A.J., Langdon, C., Albright, R., Bates, N.R., Caldeira, K., Carlton, R., Corredor, J.E., Dunbar, R.B., Enochs, I. and Erez, J., 2018. Taking the metabolic pulse of the world's coral reefs. PloS one, 13(1), p.e0190872.

Dagg, M., Benner, R., Lohrenz, S. and Lawrence, D., 2004. Transformation of dissolved and particulate materials on continental shelves influenced by large rivers: plume processes. Continental shelf research, 24(7-8), pp.833-858.

Deffeyes, K.S., 1965. Carbonate equilibria: A graphic and algebraic approach 1. Limnology and Oceanography, 10(3), pp.412-426.

De Souza Machado, A.A., Spencer, K., Kloas, W., Toffolon, M., and Zarfl, C., 2016. Metal fate and effects in estuaries: a review and conceptual model for better understanding of toxicity. Science of the Total Environment, 541, pp.268-281.

Diaz, R.J. and Solow, A., 1999. Ecological and economic consequences of hypoxia: topic 2 report for the integrated assessment on hypoxia in the Gulf of Mexico.

Diaz, R.J. and Rosenberg, R., 2008. Spreading dead zones and consequences for marine ecosystems. science, 321(5891), pp.926-929.

Dickson, A.G., Sabine, C.L. and Christian, J.R. (Eds.) 2007. Guide to best practices for ocean CO2 measurements. PICES Special Publication 3, 191 pp.

Doval, M.D. and Hansell, D.A., 2000. Organic carbon and apparent oxygen utilization in the western South Pacific and the central Indian Oceans. Marine Chemistry, 68(3), pp.249-264.

Eleuterius, C.K., and Criss, G.A., 1994. St. Louis Bay Hydrology and Selected Chemistry with Data Appendix. The University of Southern Mississippi, Gulf Coast Research Laboratory, Physical Oceanography.

Engle, V.D., Summers, J.K. and Macauley, J.M., 1999. Dissolved oxygen conditions in northern Gulf of Mexico estuaries. Environmental Monitoring and Assessment, 57(1), pp.1-20.

Feng, Y., Fennel, K., Jackson, G.A., DiMarco, S.F. and Hetland, R.D., 2014. A model study of the response of hypoxia to upwelling-favorable wind on the northern Gulf of Mexico shelf. Journal of Marine Systems, 131, pp.63-73.

Fichot, C.G., and Benner, R., 2012. The spectral slope coefficient of chromophoric dissolved organic matter (S275–295) as a tracer of terrigenous dissolved organic carbon in river-influenced ocean margins. Limnology and Oceanography, 57(5), pp.1453-1466.

Flemer, D.A., Kruczynski, W.L., Ruth, B.F. and Bundrick, C.M., 1998. The relative influence of hypoxia, anoxia, and associated environmental factors as determinants of macrobenthic community structure in northern Gulf of Mexico estuary. Journal of Aquatic Ecosystem Stress and Recovery, 6(4), pp.311-327.

Fowler, R.A., Saros, J.E. and Osburn, C.L., 2018. Shifting DOC concentration and quality in the freshwater lakes of the Kangerlussuaq region: An experimental assessment of possible mechanisms. Arctic, Antarctic, and Alpine Research, 50(1), p.S100013.

Friis, K., Körtzinger, A., and Wallace, D.W., 2003. The salinity normalization of marine inorganic carbon chemistry data. Geophysical Research Letters, 30(2).

Gonzalez, J.L., Thouvenin, B. and Dance, C., 2007. The role of particles in the behavior and speciation of trace metals: the cadmium example. Houille Blanche-Revue Internationale De L Eau, (4), pp.56-62.

Guo, L., Santschi, P.H. and Warnken, K.W., 2000. Trace metal composition of colloidal organic material in marine environments. Marine Chemistry, 70(4), pp.257-275.

Guo, L., Hunt, B.J., Santschi, P.H. and Ray, S.M., 2001. Effect of dissolved organic matter on the uptake of trace metals by American oysters. Environmental science & technology, 35(5), pp.885-893.

Guo, X., Dai, M., Zhai, W., Cai, W.J. and Chen, B., 2009. CO2 flux and seasonal variability in a large subtropical estuarine system, the Pearl River Estuary, China. Journal of Geophysical Research: Biogeosciences, 114(G3).

Haitzer, M., Höss, S., Traunspurger, W. and Steinberg, C., 1998. Effects of dissolved organic matter (DOM) on the bioconcentration of organic chemicals in aquatic organisms—a review—. Chemosphere, 37(7), pp.1335-1362.

Hansell, D.A., Carlson, C.A., Repeta, D.J. and Schlitzer, R., 2009. Dissolved organic matter in the ocean: A controversy stimulates new insights. Oceanography, 22(4), pp.202-211.

Hansell, D.A. and Carlson, C.A. eds., 2014. Biogeochemistry of marine dissolved organic matter. Academic Press.

Hedges, J.I., 1992. Global biogeochemical cycles: progress and problems. Marine Chemistry, 39(1-3), pp.67-93.

Heisler, J., Glibert, P.M., Burkholder, J.M., Anderson, D.M., Cochlan, W., Dennison, W.C., Dortch, Q., Gobler, C.J., Heil, C.A., Humphries, E. and Lewitus, A., 2008. Eutrophication and harmful algal blooms: a scientific consensus. Harmful algae, 8(1), pp.3-13.

Helms, J.R., Stubbins, A., Ritchie, J.D., Minor, E.C., Kieber, D.J. and Mopper, K., 2008. Absorption spectral slopes and slope ratios as indicators of molecular weight, source, and photobleaching of chromophoric dissolved organic matter. Limnology and Oceanography, 53(3), pp.955-969.

Hernes, P.J. and Benner, R., 2003. Photochemical and microbial degradation of dissolved lignin phenols: Implications for the fate of terrigenous dissolved organic matter in marine environments. Journal of Geophysical Research: Oceans, 108(C9).

Hetland, R.D. and DiMarco, S.F., 2008. How does the character of oxygen demand control the structure of hypoxia on the Texas–Louisiana continental shelf?. Journal of Marine Systems, 70(1-2), pp.49-62.

Ho, P., Shim, M.J., Howden, S.D. and Shiller, A.M., 2019. Temporal and spatial distributions of nutrients and trace elements (Ba, Cs, Cr, Fe, Mn, Mo, U, V, and Re) in Mississippi coastal waters: Influence of hypoxia, submarine groundwater discharge, and episodic events. Continental Shelf Research, 175, pp.53-69.

Hudson, N., Baker, A. and Reynolds, D., 2007. Fluorescence analysis of dissolved organic matter in natural, waste and polluted waters—a review. River research and applications, 23(6), pp.631-649.

Joung, D. and Shiller, A.M., 2016. Temporal and spatial variations of dissolved and colloidal trace elements in Louisiana Shelf waters. Marine Chemistry, 181, pp.25-43.

Joshi, I. and D'Sa, E., 2015. Seasonal variation of colored dissolved organic matter in Barataria Bay, Louisiana, using combined Landsat and field data. Remote Sensing, 7(9), pp.12478-12502.

Kawahata, H., Suzuki, A. and Goto, K., 1997. Coral reef ecosystems as a source of atmospheric CO2: Evidence from pCO2 measurements of surface waters. Coral Reefs, 16(4), pp.261-266.

Kalbitz, K., Solinger, S., Park, J.H., Michalzik, B. and Matzner, E., 2000. Controls on the dynamics of dissolved organic matter in soils: a review. *Soil science, 165*(4), pp.277-304.

Keith, D., Lunetta, R. and Schaeffer, B., 2016. Optical models for remote sensing of colored dissolved organic matter absorption and salinity in New England, Middle Atlantic and gulf coast Estuaries USA. Remote Sensing, 8(4), p.283.

Kirk, J.T., 1988. Solar heating of water bodies as influenced by their inherent optical properties. Journal of Geophysical Research: Atmospheres, 93(D9), pp.10897-10908.

LaFond, E.C., 1954. Factors affecting vertical temperature gradients in the upper layers of the sea. The Scientific Monthly, 78(4), pp.243-253.

Lenihan, H., Peterson, C.S., Grassle, J.P., Kelsey, A., Oates, E., and Snelgrove, P.V., 1995, March. Mass mortality of oysters, Crassostrea virginica, in a wind-driven estuary: Prolonged hypoxia and the restoration of a declining fishery. In Benthic Ecology Meeting Summary. New Brunswick, NJ (pp. 17-19).

Lin, P., Chen, M. and Guo, L., 2012. Speciation and transformation of phosphorus and its mixing behavior in the Bay of St. Louis estuary in the northern Gulf of Mexico. Geochimica et Cosmochimica Acta, 87, pp.283-298.

Lin, V.S., 2015. Research highlights: challenges in the characterization, storage, and isolation of natural organic matter. Environmental Science: Processes & Impacts, 17(12), pp.2002-2005.

Macdonald, R.W., Carmack, E.C., McLaughlin, F.A., Iseki, K., Macdonald, D.M. and O'Brien, M.C., 1989. Composition and modification of water masses in the Mackenzie Shelf Estuary. Journal of Geophysical Research: Oceans, 94(C12), pp.18057-18070.

Matsuoka, A., Bricaud, A., Benner, R., Para, J., Sempéré, R., Prieur, L., Bélanger, S. and Babin, M., 2012. Tracing the transport of colored dissolved organic matter in water masses of the Southern Beaufort Sea: relationship with hydrographic characteristics. Biogeosciences, 9(3), p.925.

Matsuoka, A., Ortega-Retuerta, E., Bricaud, A., Arrigo, K.R. and Babin, M., 2015. Characteristics of colored dissolved organic matter (CDOM) in the Western Arctic Ocean: relationships with microbial activities. Deep Sea Research Part II: Topical Studies in Oceanography, 118, pp.44-52.

Mattsson, T., Kortelainen, P., Laubel, A., Evans, D., Pujo-Pay, M., Räike, A. and Conan, P., 2009. Export of dissolved organic matter in relation to land use along a European climatic gradient. Science of the Total Environment, 407(6), pp.1967-1976.

Meybeck, M., 1982. Carbon, nitrogen, and phosphorus transport by World Rivers. Am. J. Sci, 282(4), pp.401-450.

Miller, W.L. and Zepp, R.G., 1995. Photochemical production of dissolved inorganic carbon from terrestrial organic matter: Significance to the oceanic organic carbon cycle. Geophysical Research Letters, 22(4), pp.417-420.

Miller, W.L. and Moran, M.A., 1997. Interaction of photochemical and microbial processes in the degradation of refractory dissolved organic matter from a coastal marine environment. Limnology and Oceanography, 42(6), pp.1317-1324.

Miller, J.L., Goodberlet, M.A. and Zaitzeff, J.B., 1998. Airborne salinity mapper makes debut in the coastal zone. Eos, Transactions American Geophysical Union, 79(14), pp.173-177.

Miller, W.L., 1998. Effects of UV radiation on aquatic humus: photochemical principles and experimental considerations. In Aquatic humic substances (pp. 125-143). Springer, Berlin, Heidelberg.

Mojzis, A.K., 2010. Explaining the variability of free-living and attached Bacterioplankton abundances in the Bay of St. Louis, Mississippi.

Moran, M.A., Sheldon, W.M. and Zepp, R.G., 2000. Carbon loss and optical property changes during long-term photochemical and biological degradation of estuarine dissolved organic matter. *Limnology and Oceanography*, *45*(6), pp.1254-1264.

Moran, M.A., Sheldon, W.M. and Zepp, R.G., 2000. Carbon loss and optical property changes during long-term photochemical and biological degradation of estuarine dissolved organic matter. Limnology and Oceanography, 45(6), pp.1254-1264.

Mostofa, K.M., Liu, C.Q., Mottaleb, M.A., Wan, G., Ogawa, H., Vione, D., Yoshioka, T. and Wu, F., 2013. Dissolved organic matter in natural waters. In Photobiogeochemistry of Organic Matter (pp. 1-137). Springer, Berlin, Heidelberg.

Nelson, B.W., Sasekumar, A. and Ibrahim, Z.Z., 1994. Neap-spring tidal effects on dissolved oxygen in two Malaysian estuaries. Hydrobiologia, 285(1-3), pp.7-17.

Obenour, D.R., Scavia, D., Rabalais, N.N., Turner, R.E. and Michalak, A.M., 2013. Retrospective analysis of midsummer hypoxic area and volume in the northern Gulf of Mexico, 1985–2011. Environmental science & technology, 47(17), pp.9808-9815.

Pan, K. and Wang, W.X., 2012. Trace metal contamination in estuarine and coastal environments in China. Science of the total environment, 421, pp.3-16.

Rabalais, N.N. and Turner, R.E., 2001. Coastal hypoxia: consequences for living resources and ecosystems. American Geophysical Union.

Rabalais, N.N., Turner, R.E. and Wiseman Jr, W.J., 2002. Gulf of Mexico hypoxia, aka "The dead zone". Annual Review of Ecology and Systematics, 33(1), pp.235-263.

Rabalais, N.N., Turner, R.E., Dortch, Q., Justic, D., Bierman, V.J. and Wiseman, W.J., 2002. Nutrient-enhanced productivity in the northern Gulf of Mexico: past, present, and future. In Nutrients and Eutrophication in Estuaries and Coastal Waters (pp. 39-63). Springer, Dordrecht.

Radke, L.C., 2002. Water allocation and critical flows: potential ionic impacts on estuarine organisms. In Proceedings of Coast to Coast (pp. 367-370).

Riebesell U., Fabry V. J., Hansson L. & Gattuso J.-P. (Eds.), 2010. Guide to best practices for ocean acidification research and data reporting, 260 p. Luxembourg: Publications Office of the European Union.

Sankar, M.S., Dash, P., Singh, S., Lu, Y., Mercer, A.E. and Chen, S., 2019. Effect of photo-biodegradation and biodegradation on the biogeochemical cycling of dissolved organic matter across diverse surface water bodies. Journal of Environmental Sciences, 77, pp.130-147.

Santos, I.R., Burnett, W.C., Dittmar, T., Suryaputra, I.G. and Chanton, J., 2009. Tidal pumping drives nutrient and dissolved organic matter dynamics in a Gulf of Mexico subterranean estuary. Geochimica et Cosmochimica Acta, 73(5), pp.1325-1339.

Sawant, P.A., 2009. Factors influencing the environmental quality of the Bay of Saint Louis, Mississippi, and implications for evolving coastal management policies.

Schlesinger, W.H. and Melack, J.M., 1981. Transport of organic carbon in the world's rivers. Tellus, 33(2), pp.172-187.

Seritti, A., Manca, B.B., Santinelli, C., Murru, E., Boldrin, A. and Nannicini, L., 2003. Relationships between dissolved organic carbon (DOC) and water mass structures in the Ionian Sea (winter 1999). Journal of Geophysical Research: Oceans, 108(C9).

Shang, P., Lu, Y., Du, Y., Jaffé, R., Findlay, R.H. and Wynn, A., 2018. Climatic and watershed controls of dissolved organic matter variation in streams across a gradient of agricultural land use. Science of the Total Environment, 612, pp.1442-1453.

Singh, S., Dash, P., Silwal, S., Feng, G., Adeli, A. and Moorhead, R.J., 2017. Influence of land use and land cover on the spatial variability of dissolved organic matter in multiple aquatic environments. Environmental Science and Pollution Research, 24(16), pp.14124-14141.

Sinsabaugh, R.L. and Foreman, C.M., 2003. Integrating dissolved organic matter metabolism and microbial diversity: an overview of conceptual models. In Aquatic Ecosystems(pp. 425-454). Academic Press.

Stanley, E.H., Powers, S.M., Lottig, N.R., Buffam, I. and Crawford, J.T., 2012. Contemporary changes in dissolved organic carbon (DOC) in human-dominated rivers: is there a role for DOC management?. Freshwater Biology, 57, pp.26-42.

Suzuki, A. and Kawahata, H., 2003. Carbon budget of coral reef systems: an overview of observations in fringing reefs, barrier reefs, and atolls in the Indo-Pacific regions. Tellus B: Chemical and Physical Meteorology, 55(2), pp.428-444

Thingstad, T.F., and Rassoulzadegan, F., 1999. Conceptual models for the biogeochemical role of the photic zone microbial food web, with particular reference to the Mediterranean Sea. Progress in Oceanography, 44(1-3), pp.271-286.

Timko, S.A., Maydanov, A., Pittelli, S.L., Conte, M.H., Cooper, W.J., Koch, B.P., Schmitt-Kopplin, P. and Gonsior, M., 2015. Depth-dependent photodegradation of marine dissolved organic matter. Frontiers in Marine Science, 2, p.66.

Tranvik, L.J., 1990. Bacterioplankton growth on fractions of dissolved organic carbon of different molecular weights from humic and clear waters. Appl. Environ. Microbiol., 56(6), pp.1672-1677.

Vodacek, A., Blough, N.V., DeGrandpre, M.D. and Nelson, R.K., 1997. Seasonal variation of CDOM and DOC in the Middle Atlantic Bight: Terrestrial inputs and photooxidation. Limnology and Oceanography, 42(4), pp.674-686.

Wang, W.X. and Guo, L., 2000. Influences of natural colloids on metal bioavailability to two marine bivalves. Environmental science & technology, 34(21), pp.4571-4576.

Wang, X., Cai, Y. and Guo, L., 2010. Preferential removal of dissolved carbohydrates during estuarine mixing in the Bay of Saint Louis in the northern Gulf of Mexico. Marine Chemistry, 119(1-4), pp.130-138.

Wanninkhof, R., Barbero, L., Byrne, R., Cai, W.J., Huang, W.J., Zhang, J.Z., Baringer, M. and Langdon, C., 2015. Ocean acidification along the Gulf Coast and East Coast of the USA. Continental Shelf Research, 98, pp.54-71.

Wershaw, R.L., 2004. Evaluation of conceptual models of natural organic matter (humus) from a consideration of the chemical and biochemical processes of humification.

Williams, C.J., Yamashita, Y., Wilson, H.F., Jaffé, R. and Xenopoulos, M.A., 2010. Unraveling the role of land use and microbial activity in shaping dissolved organic matter characteristics in stream ecosystems. Limnology and Oceanography, 55(3), pp.1159-1171.

CHAPTER IV

CONCLUSIONS

Two algorithms were developed for the hyperspectral sensor, nano-hyperspec, and one algorithm was developed for the multispectral sensor, RedEdge, successfully for estimating CDOM using UAS imagery over the Henderson Point and Pass Christian Oyster reefs, together which make the largest oyster reef along western Mississippi Sound in northern Gulf of Mexico. Observed DOM dynamics showed a seasonal variation pattern due to the freshwater input, which strongly influence the biogeochemical processes in the study area. Higher a_{CDOM} values were reported in spring season associated with a peak discharge from WR and JR while low a_{CDOM} observed in summer with low freshwater inputs. The observed CDOM absorption spectral slopes were high in summer and low in spring; suggesting the influence larger organic molecules during higher discharge. The measured hyperspectral and multispectral data were used to develop empirical R_{rs} algorithms to retrieve a_{CDOM} remotely. Three successful algorithms were developed by selecting R_{rs} at 482, 490, 520, 663, and 670 nm bands in the visible region of the electromagnetic spectrum. Accuracy of the algorithms increased when the seasonal variability was accounted for. A Power-law functional form with band ratio produced best algorithms for the hyperspectral data with R^2 of 0.70 and 0.75). The multispectral algorithm had a higher R^2 of 0.81 than the algorithms developed for the hyperspectral sensor.

Seasonal impact of physical and biogeochemical parameters on DOM dynamics was studied using a suite of measured parameters including salinity, pH, DO, DOC, and DIC in the

study area. A comparison of spring and summer data indicated the seasonal variation in quality and quantity of DOM in the study area. The observed nDIC and n*TAlk* suggest the respiration and dissolution activities were predominant in the spring season whereas photosynthesis and calcification processes were predominant during the summer season. These primary mechanisms can control the quality and quantity of organic and inorganic carbon in the water column, which directly affect the distribution of DOM. The direct influence of organic carbon metabolism, including photosynthesis and CO_2 respiration and inorganic carbon metabolism together with calcification and dissolution of carbonate affects the oyster reefs significantly in the study area.

Both physical and biogeochemical processes control the occurrence of hypoxic conditions in the study area. Potential hypoxic conditions appear due to the availability of organic matter to respire with the presence of favorable physical conditions during summer. This study reveals the possible implications which can lead to hypoxic conditions over the Henderson Point and Pass Christian Oyster reefs. Similarly, distribution of trace metals (e.g., As, Sb, U, Co, and Ni) in surface waters showed a conservative mixing pattern. Additionally, the availability of organic matter enhances the bioaccumulation of these trace metals in aquatic species. Physical and biogeochemical variabilities are highly sensitive to the seasonal changes. Hence, frequent water quality monitoring is required and remote sensing is best suited to monitor these changes in water quality. A time-series analysis of water quality parameters will provide important information about the source, transport, and fate of water quality parameters, which is essential for management purposes.

APPENDIX A

TRACE METAL VARIATION WITH SALINITY

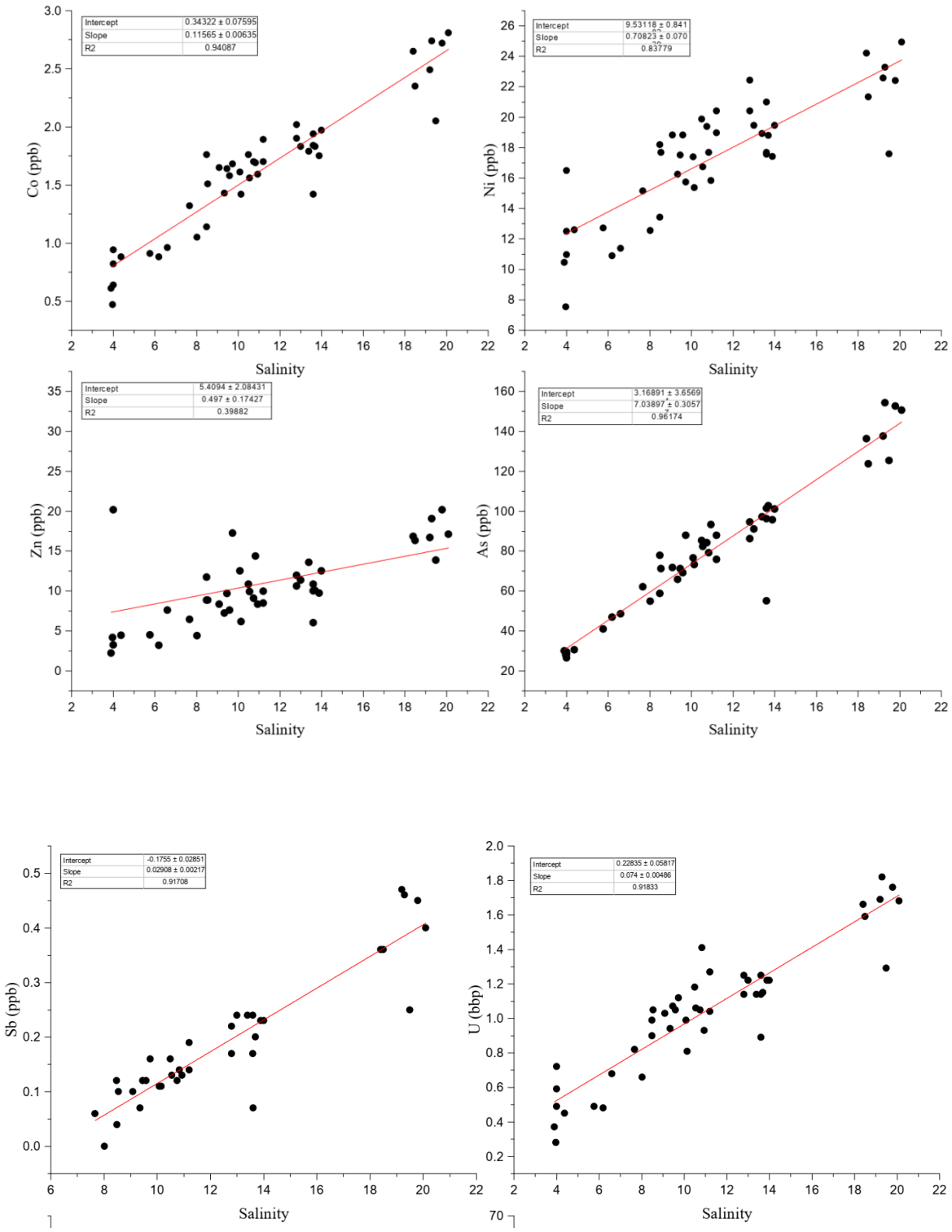

Figure A.1 Variation of trace metal with respect to salinity for the study area (samples were collected during March, May, June and July 2018.

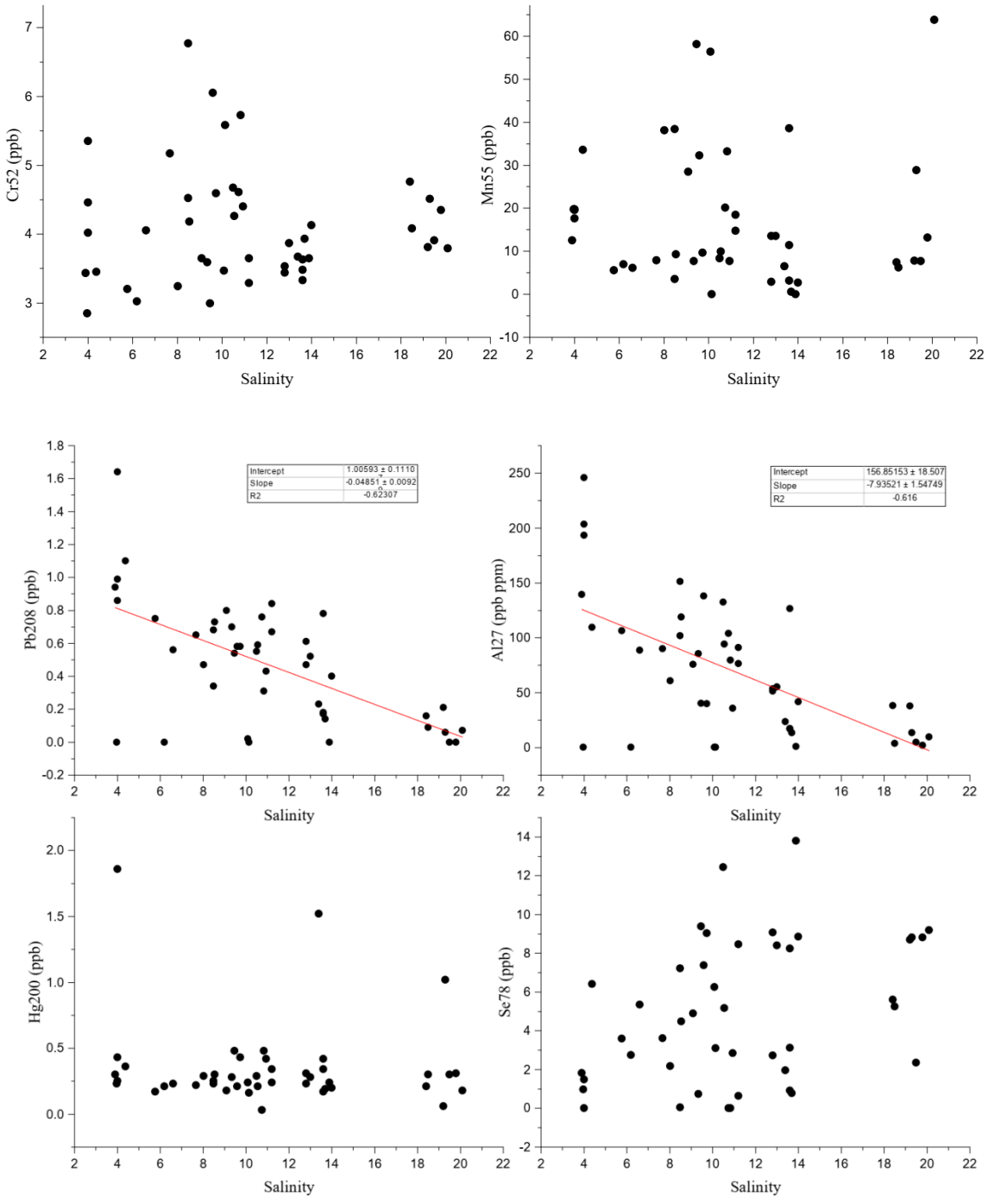

Figure A.1 (continued)